N78-32596

NASA Contractor Report 158945

Aircraft HO_x and NO_x Emission Effects on Stratospheric Ozone and Temperature

L. Glatt and G. F. Widhopf

THE AEROSPACE CORPORATION
EL SEGUNDO, CA 90245

CONTRACT NAS1-13970
SEPTEMBER 1978

National Aeronautics and
Space Administration

Langley Research Center
Hampton, Virginia 23665

NASA Contractor Report 158945

AIRCRAFT HO_x AND NO_x EMISSION EFFECTS ON STRATOSPHERIC OZONE AND TEMPERATURE

By L. Glatt and G. F. Widhopf

The Aerospace Corporation
El Segundo, CA 90245

NATIONAL AERONAUTICS AND SPACE ADMINISTRATION

AIRCRAFT HO_x AND NO_x EMISSION EFFECTS ON STRATOSPHERIC OZONE AND TEMPERATURE

By L. Glatt and G. F. Widhopf
The Aerospace Corporation

SUMMARY

A simplified two-dimensional steady-state photochemical model of the atmosphere, which includes the effects of atmosphere radiation, has been developed to investigate the effect of injection of NO_x and HO_x on the chemical and thermal structure of the stratosphere.

The model has been developed in two parts. The first part is the development of the natural atmosphere, and is characterized by the coupled solution of the energy and the species conservation equations in the stratosphere with the temperature of the natural atmosphere prescribed. The results of this calculation are a coupled solution for the meridional circulation and the chemical structure of the natural atmosphere. Included in this model is the development of an active water vapor model that accounts for convection, diffusion, rainout/washout and chemistry. The model of the natural atmosphere has been run for the fall season, and the water vapor distributions are in good agreement with available data.

The second part consists of the development of a model of the perturbed atmosphere and is characterized by the solution of the coupled energy and species conservation equations. In this model, the meridional circulation is prescribed from solution of the natural atmosphere and the energy equation is solved for the temperature perturbation resulting from the injection of NO_x and HO_x pollutants. The model has been used to study the effect on the thermal and chemical structure of the atmosphere of two types of pollution cases: (a) injection of NO_x and HO_x from a hypothetical fleet of supersonic and subsonic aircraft and (b) injection of HO_x from a hypothetical fleet of liquid-fueled hydrogen aircraft. The results are discussed with regard to stratospheric perturbations in ozone, water vapor and temperature.

INTRODUCTION

The effect of aircraft pollutants on the state of the atmosphere, especially the ozone layer, has been the subject of intense investigation for a number of years. In order to study this problem, photochemical models of the atmosphere have been developed together with making measurements

of various stratospheric properties. Both of these efforts have led to a better understanding of various stratospheric phenomena together with providing numerical atmospheric models that can make state-of-the-art estimates of the potential effect of high flying aircraft on the ozone layer.

Atmospheric models have progressed from the most simple box model to more sophisticated one-dimensional and multidimensional models. Due to the complexity of the physical problems, these models have progressed in steps, developing better phenomenology for describing various atmospheric phenomena at each step. In all models, various aspects of the overall problem have been either neglected or modeled in a very simple manner. In general, the most important phenomena have been included in these models and, as a result of continued development some of the initial approximations have been relaxed. The work reported herein attempts to relax some of the constraints of previous models, specifically the omission of active water vapor transport and the uncoupling of the stratospheric temperature distribution from changes in atmospheric species concentration. These temperature and species concentration changes can result from the introduction of pollutants in the stratosphere and are of interest because of the feedback influence these temperature and species concentration perturbations can have on chemical rate processes, mean atmospheric transport and climate.

This coupling was initially investigated by Ramanathan (ref. 1) using a one-dimensional radiative-convective (radiative equilibrium) model. A two-dimensional coupled circulation model of the stratosphere, incorporating the effects of radiation, photochemistry and seasonal transport processes, was developed by Rao (ref. 2). This model was used to study the natural atmosphere and to investigate ozone and temperature perturbations due to NO_x emissions from a fleet of supersonic aircraft flying at 20 km and 45°N in the summer hemisphere (ref. 3). However, active water vapor was not included in either of these studies, and only a very simple radiation model was used by Rao.

Active water vapor transport is of interest for many reasons and has been investigated only recently with limited success. In order to adequately calculate the water vapor distribution in the natural atmosphere, the dynamic interchange between the troposphere and stratosphere, together with the rainout/washout mechanisms in the troposphere, must be considered. In the initial stage of development, multidimensional models were not able to handle active water vapor transport; thus, the problem was circumvented by specifying the water vapor distributions using available measurements. This, however, did not allow for an active means for treating the HO_x pollution problem. This pollution problem has become much more important in recent years in determining the effect of aircraft exhaust emissions on the chemical and thermal structure of the atmosphere. This is a consequence of the importance of the species OH and the measurement of new reaction rates that increase the relative importance of HO_x with respect to NO_x on the distribution of ozone.

The work to be described in this report consists of the development of a simplified two-dimensional, coupled, radiation-species model of the atmosphere. Basically, it is a modification of an existing phenomenological photochemical model of the atmosphere developed at The Aerospace Corporation (ref. 4). Due to the limited nature of one-dimensional models, it is desirable to have the same technology available in a multidimensional model in order to more realistically determine any associated effects of pollutants. This is required since the more realistic transport and strong latitudinal gradients in temperature, density and solar flux present in a two-dimensional model can influence the magnitude and distribution of the resulting atmospheric perturbations.

The development of this capability requires the solution of the energy equation, which is a balance between the advective and turbulent diffusive transport of heat and the radiative heating/cooling. In this study, the local radiation flux is evaluated using a comprehensive simplified model developed by Ramanathan (ref. 1). The advective transport of heat is evaluated by calculating the meridional wind field. Since the calculation of the meridional circulation from the governing continuity and momentum equations is very time-consuming, due to numerical time step limitations, an approximate method is used. This method utilizes the continuity and energy equations to solve for the meridional velocity components. Since the energy equation is also utilized to calculate temperature changes, it is apparent that both the temperature and the wind field cannot be computed simultaneously. The procedure in this work is to evaluate the meridional circulation in the natural atmosphere and then hold it fixed in the perturbed atmosphere using the energy equation to compute temperature changes in this case.

In order to make these calculations self-consistent, the same radiation model must be used to compute both the circulation and temperature perturbations. Before the radiation model is used, a two-dimensional evaluation of the validity of this model is performed. The calculation of the meridional circulation patterns and various aspects of using this approximate method are also discussed. These results are compared to a similar calculation performed by Louis (ref. 5) whose circulation patterns were originally used in the basic model developed previous to this work. Some inert tracer experiments performed using these resulting circulation patterns are described as well and compared to available data.

A discussion of the water vapor transport model is included, as well as a description of the coupled species-circulation-radiation model of the natural atmosphere. Here, the energy, species and continuity equations were solved simultaneously using prescribed meridional temperature distributions compiled from data by Louis (ref. 5). The Aerospace atmospheric model which was used as a basis for the incorporation of these changes is described in the Appendix. Typical results of this coupled calculation of the natural atmosphere are also presented.

In order to evaluate the effect of HO_x and NO_x on the atmospheric distribution of various species concentrations and the temperature distribution, the meridional circulation calculated in the natural atmosphere is held fixed,

and the energy equation is used to solve for the associated temperature changes. This procedure does not allow for an estimate of the effect of the species concentration change on the circulation patterns, and therefore yields an upper limit estimate of the temperature changes.

Two aircraft pollution cases are investigated. The first is an injection of NO_x and HO_x from a combined fleet of subsonic and supersonic aircraft flying in the troposphere and stratosphere. The second case considers a hypothetical fleet of liquid hydrogen-fueled aircraft cruising at 20.6 km. The results of these calculations are discussed in regard to perturbations in ozone and stratospheric temperature.

SYMBOLS

A_o	time constant for rainout in troposphere, s^{-1}
c_p	specific heat at constant pressure, $cm^2/s^2\text{-}^oK$
e_s	saturation vapor pressure, atm
F_o	energy source/sink distribution, $^oK/day$
F'	perturbation of energy source/sink distribution, $^oK/day$
$G(z)$	function defined by equation (8)
H	height of troposphere
$H(\phi)$	function defined by equation (8)
h	relative humidity
K_{ij}	turbulent eddy diffusivity tensor, km^2/s
K_o	coefficient of vertical eddy diffusion in troposphere, (K_{zz}), km^2/s
p	pressure, atm
p_o	reference pressure, atm
$\dot{Q}_E$	turbulent diffusion of heat, $^oK/day$
$\dot{Q}_R$	radiative heating, $^oK/day$
R	gas constant for air, $cm^2/s^2\text{-}^oK$
$\overline{R}$	function defined by equation (7)
r	vertical distance from center of earth, km

T	atmospheric temperature, ^{o}K
v	meridional velocity, km/s
w	vertical velocity, km/s
Y_i	mass fraction of species i
z	vertical distance from earth surface, km
$\bar{z}$	z/H
ϕ	latitude, degrees
θ	potential temperature, ^{o}K
ρ	atmospheric density, gm/cm^3
π	reduced pressure $(p/p_o)^{R/c_p}$
$\bar{\lambda}$	$H\sqrt{A_o/K_o}$

Subscripts:

*	surface value

Superscripts:

( )'	perturbed value

RADIATION MODELING

The solution of the energy equation for the temperature perturbations or alternatively for the meridional circulation requires the distribution of radiative sources and sinks in the atmosphere. In this regard, a simplified, yet comprehensive and realistic radiation model of the atmosphere, developed by Ramanathan (ref. 1) was utilized in the present study. The model considers the stratospheric radiative transfer due to H_2O, CO_2 and O_3. It includes solar absorption by six bands of water vapor in the region 0.9μ - 6.3μ, by ten bands of CO_2 in the regions 2.0μ, 2.7μ and 4.3μ, and also the ultraviolet and visible absorption bands of ozone. In addition, the model treats long wavelength radiation by the vibration-rotation, pure rotation and two continuum bands of water vapor, the 9.6μ band of ozone and the four fundamental and six hot bands of CO_2. Specific details of the model are discussed by Ramanathan (ref. 1).

At the initiation of this study, this radiation model had been included only in a one-dimensional model, and thus it was necessary to determine whether the model could predict the meridional distribution of radiative

heating/cooling reasonably well. As a test, the model results were compared with the results of a more comprehensive model developed by Dopplick (ref. 6). In this context, it must be emphasized that the atmospheric distribution of radiative parameters (i.e., temperature, cloud cover, ozone and H_2O distributions) was not identical in both calculations. For this verification study, the temperature field was taken from the data compilations of Louis (ref. 5), the ozone distributions from Wilcox, Nastrom and Belmont (ref. 7), and the tropospheric water vapor from Manabe and Wetherald (ref. 8). The stratospheric water vapor mass mixing ratio was assumed to be 2.5 ppm.

The initial results for the meridional distribution of radiative heating/cooling rates were not in good agreement with Dopplick's results. After careful analysis of these results, it was found that the disagreement was due to the method in which the solar flux was evaluated. The solar heating flux was evaluated in the original radiation model using an average daylight value of the cosine of the solar zenith angle. This model does not properly evaluate the diurnally averaged solar radiation needed in a two-dimensional application. To correct this aspect of the model, it was necessary to integrate the solar radiation flux over a 24-hour period. The results obtained after the above modification was incorporated in the model are shown in figure 1a and compared with those of Dopplick (fig. 1b) for the fall season (where the fall season refers to the northern hemisphere). Dopplick's calculations were available only below 32 km, whereas the present calculations were performed for the region 15-50 km. The present calculations were limited to altitudes above 15 km, since the present radiation model is not valid in the troposphere. Comparison of figures 1a and 1b shows good agreement between the two methods in the region 15-32 km. Figures 2 through 4 show the results of the net radiative heating rates for the winter, spring and summer seasons, respectively, which, although not shown, are also in good agreement with Dopplick's results.

Thus, the radiation model developed by Ramanathan provides an adequate description of the stratospheric radiative sources and sinks in the natural atmosphere, provided the diurnally averaged solar flux is evaluated properly. Because of its simplicity, it is well suited for use in a photochemical model of the atmosphere. In this regard, it can be used to evaluate the required radiative contribution in the energy equation for the solution of either the meridional circulation or the temperature perturbations.

MERIDIONAL CIRCULATION

The computation of the meridional circulation by solving the primitive equations can be very time-consuming, primarily due to the requirement of a small time step in order to insure that a stable numerical solution is obtained. For this reason, approximate methods have been developed. In general, these methods reduce the number of partial differential equations to two. These two equations are solved for the horizontal (v) and vertical (w) components of the meridional circulation, with the remaining variables

such as density and temperature prescribed. In most cases, one of the equations is the continuity equation, whereas the second is either the energy equation [Murgatroyd, et al. (ref. 9) and Louis (ref. 5)] or the zonal momentum equation [Vincent (ref. 10)]. The two-dimensional Aerospace Corporation model used as a basis for the present investigation originally employed the meridional circulation patterns computed by Louis (ref. 5). However, because of the differences in the radiation and turbulent diffusion models used by Louis and that used in the present work, the meridional circulation patterns must be recalculated. This is necessary in order to obtain a consistent evaluation of the energy equation that will allow a determination of temperature perturbations resulting from the introduction of pollutants into the stratosphere.

The method used in the present calculation follows along the lines of Louis (ref. 5). The major differences in the computation of the meridional circulation are the methods in which the radiative heating and eddy flux of sensible heat are modeled. The following paragraphs outline the basic equations and the method used in computing the seasonal circulation.

The basic equations are the energy equation

$$\frac{\partial \theta}{\partial t} + \frac{v}{r}\frac{\partial \theta}{\partial \phi} + w\frac{\partial \theta}{\partial z} = \dot{Q}_E + \frac{\dot{Q}_R}{\pi} \tag{1}$$

and the continuity equation

$$\frac{\partial \rho}{\partial t} + \frac{1}{r\cos\phi}\frac{\partial}{\partial \phi}(\rho v \cos\phi) + \frac{\partial}{\partial z}(\rho w) = 0 \tag{2}$$

where θ is the potential temperature, $\pi = (p/p_o)^{R/c_p}$ is the reduced pressure, ρ is the density, v, w are the meridional and vertical velocity components, respectively, and $T \equiv \theta\pi$. The terms $\dot{Q}_E$ and $\dot{Q}_R$ are the diabatic heating terms due to turbulent diffusion and radiation, respectively. The heating due to radiation is computed using the model developed by Ramanathan (ref. 1) as described in the previous section. The heating due to the turbulent eddy flux is computed using an eddy diffusivity model [see Reed and German (ref. 11)] and is given by

$$\begin{aligned}\dot{Q}_E = {} & \frac{1}{r}\frac{\partial}{\partial \phi}\left(\frac{K_{\phi\phi}}{r}\frac{\partial \theta}{\partial \phi}\right) + \frac{\partial}{\partial z}\left(K_{zz}\frac{\partial \theta}{\partial z}\right) + \frac{1}{r}\frac{\partial}{\partial \phi}\left(K_{\phi z}\frac{\partial \theta}{\partial z}\right) \\ & + \frac{\partial}{\partial z}\left(\frac{K_{z\phi}}{r}\frac{\partial \theta}{\partial \phi}\right) + \frac{2}{r}\left[K_{zz}\frac{\partial \theta}{\partial z} + \frac{K_{z\phi}}{r}\frac{\partial \theta}{\partial \phi}\right] \\ & - \frac{\tan\phi}{r}\left[K_{\phi z}\frac{\partial \theta}{\partial z} + \frac{K_{\phi\phi}}{r}\frac{\partial \theta}{\partial \phi}\right]\end{aligned} \tag{3}$$

where K_{ij} is the given eddy diffusivity tensor. The specific components of K_{ij} used in this computation are those developed by Luther (ref. 12) and modified by Glatt and Widhopf (ref. 13). In the above model, we have accounted for both the horizontal and vertical flux contributions to the turbulent heating. For the calculation of the meridional circulation, the potential temperature and density are given. Thus, equation (1) can be written as

$$\frac{v}{r}\frac{\partial \theta}{\partial \phi} + w\frac{\partial \theta}{\partial z} \equiv F_o(z,\phi) = \dot{Q}_E + \frac{\dot{Q}_R}{\pi} - \left(\frac{\partial \theta}{\partial t}\right)_{season} \tag{4}$$

where F_o represents the distribution of energy sources and sinks. As pointed out by Louis (ref. 5), the term $\partial\rho/\partial t$ in the continuity equation is at least two orders of magnitude smaller than the other terms and thus can be neglected. Therefore, equation (2) becomes

$$\frac{1}{r\cos\phi}\frac{\partial}{\partial \phi}(\rho v \cos\phi) + \frac{\partial}{\partial z}(\rho w) = 0 \tag{5}$$

Equations (4) and (5) can now be solved for v and w. Although the computation of v and w is straightforward, the computed values of w must satisfy

$$\int_{-\pi/2}^{\pi/2} \rho w \cos\phi \, d\phi = 0 \tag{6}$$

since $v = 0$ at both poles.

Since the method is only approximate, equation (6) generally will not be satisfied. Thus, an iterative procedure is required which allows the function F_o to be perturbed in order to satisfy equation (6). The sequential steps of the solution procedure are:

(1) Solve for w from equation (4).

(2) Compute v from equation (5).

(3) Evaluate the left-hand side of equation (6).

(4) Perturb F_o by $F'(z,\phi)$ so that the w computed by equation (4) with the latest values of v satisfies equation (6).

(5) Recompute v from equation (5) using the new values of w computed in equation (4).

(6) Repeat steps (4) and (5) until the values of v at consecutive interations differ by a given ϵ.

Since equation (6) is an integral constraint on w, there exist many choices for $F'(z,\phi)$ which will satisfy this integral constraint. Thus, the problem of nonuniqueness of the meridional circulation can exist when this method is used. A sensitivity study has been performed to assess the effect of varying F' on the computed winds; the results will be discussed later.

By satisfying equation (6), we require

$$\int_{-\pi/2}^{\pi/2} \left[\frac{\rho F'}{\partial\theta/\partial z}\right] \cos\phi \; d\phi = - \int_{-\pi/2}^{\pi/2} \frac{\rho\left[F_o - \frac{v}{r}\frac{\partial\theta}{\partial\phi}\right]}{\partial\theta/\partial z} \cos\phi \; d\phi \equiv \overline{R} \tag{7}$$

To simplify the integration, we assume $\rho F'/(\partial\theta/\partial z)$ can be separated into the product of two functions, one a function of z and the other a function of ϕ, i.e.,

$$\frac{\rho F'}{\partial\theta/\partial z} = G(z)\, H(\phi) \tag{8}$$

Substituting equation (8) into the left-hand side of equation (7) and solving for $G(z)$ yields

$$G(z) = \frac{\overline{R}}{\int_{-\pi/2}^{\pi/2} H(\phi) \cos\phi \; d\phi} \tag{9}$$

When equation (9) is substituted into equation (8), the following expression for $F'(z,\phi)$ is obtained.

$$F'(z,\phi) = \frac{1}{\rho}\frac{\partial\theta}{\partial z}\left[\frac{\overline{R}\, H(\phi)}{\int_{-\pi/2}^{\pi/2} H(\phi) \cos\phi \; d\phi}\right] \tag{10}$$

The function $H(\phi)$ must now be chosen. Louis (ref. 5) selected $H(\phi) = \cos\phi$. This function concentrates the perturbation around the equator where $\cos\phi$ is unity and introduces a zero perturbation at the poles. However, since the circulation is most important, from the standpoint of transport, at latitudes less than 50°-60°, an attempt should be made to reduce the perturbation in this region. In the present analysis, $H(\phi)$ is chosen to be unity, since for this function the perturbation is evenly distributed from pole to pole. The ratio of the perturbations for the function $H(\phi) = \cos\phi$ ($\equiv F'_L$)

and $H(\phi) = 1$ ($\equiv F'$) can easily be obtained using equation (10), i.e., $F'/F'_L = \pi/(4\cos\phi)$. Thus, for $\phi \leq 45^\circ$, the perturbation using $H(\phi) = 1$ is less than or equal to that for the case $H(\phi) = \cos\phi$. This is desirable, since large perturbations are inconsistent with the method.

This method was used to calculate the meridional circulation for each of the four seasons. The required inputs to the model are θ, ρ and the concentrations of O_3, CO_2 and H_2O. The seasonal distributions of temperature [Louis (ref. 5)], which are used in the basic two-dimensional model, were utilized in this calculation. The pressure was obtained from the hydrostatic equilibrium relationship and the density calculated from the perfect gas equation of state. Using the pressure and temperature, the potential temperature can be obtained. The mass mixing ratio of CO_2 is assumed to be uniform with a value of 488 ppm [Ramanathan (ref. 1)], while the monthly ozone distributions are taken from Wilcox, Nastrom and Belmont (ref. 7).

The water vapor distribution is based on a relative humidity formulation taken from Manabe and Wetherald (ref. 8). This water vapor model was developed after careful analysis of data in the troposphere demonstrated that the meridional distribution of relative humidity was nearly similar for the different seasons and, thus, one could use the data to approximate an average relative humidity distribution. Manabe and Wetherald found the vertical distribution of relative humidity could be represented by

$$h = h_* \frac{\left(p/p_* - 0.02\right)}{1 - 0.02} \tag{11}$$

where h_* is the relative humidity at the earth's surface, p the pressure and p_* the surface pressure. When p/p_* is less than 0.02, the relative humidity becomes negative; it is therefore necessary to specify the humidity distribution for small values of p/p_*. According to the measurements of Mastenbrook (ref. 14), the stratosphere is very dry and the mixing ratio is about 2×10^{-6} gm/gm of air. Thus, the mass mixing ratio is given by

$$Y_{H_2O} = \frac{0.622h\, e_s(T)}{p - h\, e_s(T)} \tag{12}$$

and

$$\left(Y_{H_2O}\right)_{min} = 2.0 \times 10^{-6}.$$

where $e_s(T)$ is the saturation vapor pressure at temperature T.

Since the Ramanathan radiation model has a number of approximations which are only valid in the stratosphere, the model does not give an adequate representation for the tropospheric radiation. With a tropospheric radiation model not available, the coupled continuity and energy equations

could only be solved in the stratosphere (i.e., above 15 km). The meridional circulation in the troposphere was taken from the data of Newell, et al. (ref. 15). This technique was also used by Louis (ref. 5).

The meridional circulation for each of the seasons has been computed and the results shown in figures 5 through 8. In each case, the corresponding circulation as computed by Louis (ref. 5) is also shown. Comparison of the two calculations indicates similar type circulations during the winter and summer seasons (figs. 6 and 8), whereas the fall and spring seasons show appreciable differences (figs. 5 and 7). Since the results of these calculations are dependent on the modeling of the radiation, turbulent diffusion, as well as the method used to satisfy the integral constraint, it is therefore important to investigate the sensitivity of the solution to variations of modeling in these areas. These are shown for the fall season in figures 9 through 11 which depict the vertical velocity component w at $\phi = 0^{o}$, 30^{o}N and 60^{o}N latitude. The curves labeled (a) are the results obtained using the present technique. Curves (b) are the results obtained by Louis (ref. 5). Curves (c) are the results obtained using the present model with one exception; the contribution due to eddy flux [eq. (3)] is replaced with that given by Louis (ref. 5). Curves (d) are the results obtained using the present model, except that in equation (8) $H(\phi) \equiv \cos\phi$ rather than unity. Finally, curves (e) are the results obtained using the present model with $H(\phi) = \cos\phi$ and Q_E given by Louis (ref. 5).

Comparison of curves (a) and (c) shows the sensitivity of the results to the modeling of Q_E. The largest differences are seen to be at 30^{o}N. Louis used data published by Newell, et al. (ref. 15). These data are questionable due to the facts that: (1) the computed fluxes are essentially the ones due to standing eddies only, and (2) the data in the upper stratosphere only cover the western half of the northern hemisphere. In the present calculations, we have used an eddy diffusivity model to describe the eddy flux of heat [equation (3)]. This model accounts for both gradient and countergradient fluxes of heat. We should emphasize that we are not suggesting that the eddy diffusivity model predicts the fluxes of heat any more or less accurately than does the use of the data, but is one method of accounting for the eddy fluxes and is consistent with the two-dimensional diffusion coefficients used in the atmospheric model.

Comparison of curves (a) $[H(\phi) = 1]$ and (d) $[H(\phi) = \cos\phi]$ shows the so-called "nonuniqueness" in the method of satisfying the integral constraint [eq. (6)]. The smallest differences occur near $\phi = 30^{o}$N, since this is the region where the heating sources are the largest. At other locations, the strength of the sources and sinks are smaller and the perturbations become more pronounced, i.e., see $\phi = 0^{o}$, 60^{o}N. This nonuniqueness is actually a failure in the method and arises when the computed perturbations F' are no longer small when compared to F_o. For the results presented, the nonuniqueness becomes apparent at the higher altitudes (i.e., above 25 km). However, the breakdown in this region is due to the poor description of the contribution to the heating due to the eddy flux, and thus a larger F' is required to satisfy equation (6). Comparisons of curves (b) and (e) show the

sensitivity of the solution to the differences between the radiation models used in the present calculation and that of Louis (ref. 5). As previously discussed, the present computation includes a radiation model developed by Ramanathan (ref. 1) to compute the heating due to O_3, CO_2 and H_2O, whereas Louis used a number of different computer codes to account for each of the radiating species [for details, see Louis (ref. 5)]. For the present results, the largest difference occurs at $\phi = 60^{\circ}N$. In general, below 30 km, the magnitude of the radiation heating is less than 1 $^{\circ}K$/day; thus there can exist a substantial effect if the models are predicting differences on the order of tenths of a degree per day.

In general, we cannot distinctly separate out the effects of both radiation and eddy flux modeling due to the integral constraint imposed by equation (6). This is because a modification of either of the above effects will require a different perturbation to satisfy equation (6) and in a manner that may overshadow the actual local physical effects.

Short of solving the complete system of primitive equations for the circulation, these approximate methods are adequate and should suffice for the phenomenological models in which they are to be used, as long as one keeps in mind the sensitivity of the results to the technique in modeling the physical processes. Some filtering of the computed results as done by Louis (ref. 5) may also be necessary.

As a further evaluation of these computed circulation patterns, inert tracer calculations were performed for carbon-14 and tungsten-185. These results are described in the next section.

TRACER STUDIES

In order to test the present meridional circulation pattern, the dispersion of carbon-14 and tungsten-185 were calculated using the new meridional circulations computed in the previous section. Figures 12 through 14 show the measurements of carbon-14 distribution [Telegadas (ref. 16); Johnston (ref. 17)] as a function of time for the latitudes $\phi = 10^{\circ}N$, $30^{\circ}N$, and $70^{\circ}N$. Also shown are the results of the latest calculations as well as the previous results obtained using Louis' circulation [Widhopf, et al. (ref. 22)]. At $10^{\circ}N$, the latest circulation overpredicts the peak concentration of carbon-14. At $30^{\circ}N$, although the earlier profiles show the peaks occurring at 1-2 km higher as well as lower concentration below the peak, these distributions approach the data over the next year or so. At $70^{\circ}N$, a similar situation occurs; i.e., by January 1965 the calculations adequately predict the data.

Figure 15 shows the results of the tungsten-185 simulation for the peak concentration in the equatorial region for both Louis' circulation and the present circulation. Along with these results are the data obtained by Friend (ref. 18) and Gudiksen, et al. (ref. 19). Notice that the new circulation adequately simulates the decay of the peak equatorial concentration of tungsten-185 as a function of time.

It must be pointed out that the turbulent diffusion coefficients used in these calculations were those obtained by Glatt and Widhopf (ref. 13) which are modifications to the original coefficients of Luther (ref. 12). This modification involved using Louis' (ref. 5) circulation and adjusting the diffusion coefficients in the high latitude regions employing the carbon-14 data as a guide. With these new coefficients, the tungsten-185 simulation was then run. In the present calculation, the seasonal circulation was computed using these diffusion coefficients. Thus, any modifications to the diffusion coefficients to bring the present results into better agreement with the data (as was done for the carbon-14) must be performed in an iterative manner since the diffusion coefficients couple back to the calculation of the season circulation. This type of study was not within the scope of the present work. However, these tests demonstrate the adequacy of the present transport.

Before a coupled radiation-species-circulation model can be developed to study the effects of HO_x pollutants on the stratospheric ozone and temperature, a consistent model of the natural atmosphere must be developed. In particular, an adequate water vapor model must be used. The development of such a model is described in the next section.

WATER VAPOR MODELING

The investigation of the effects of HO_x pollutants on the stratospheric ozone and temperature requires an active water vapor model. This model must account for transport by meridional winds, diffusion by turbulent eddies, chemical production and/or depletion, and include the effects of evaporation and precipitation.

From a physical standpoint, a steady-state water vapor distribution can only exist if the difference between the evaporation from the surface E, and the precipitation P, integrated over the entire globe vanishes. Since the major portion of the water vapor is located in the troposphere, a tropospheric water vapor model must be developed.

Before development of a two-dimensional model is initiated, one can make use of a simplified one-dimensional model in order to determine the effects of boundary conditions, transport, chemistry and rainout on the level of water vapor. The lowest order one-dimensional model is based on the assumption that under steady-state conditions in the troposphere, a balance exists between the divergence of the vertical eddy flux and the rainout of water vapor (i.e., precipitation), with chemistry being a higher order effect. This latter assumption is subsequently verified by actual computation.

To elaborate on the model, consider a region of depth H in which both the vertical eddy diffusivity K_o and residence time A_o (i.e., the time constant for rainout) are both independent of altitude. Mathematically, the governing equation for the steady-state distribution of water vapor is given by

$$K_o \frac{d^2Y}{dz^2} - A_o Y = 0 \qquad (13)$$

where Y is the mass fraction of water vapor. The boundary conditions imposed on equation (13) are

$$Y(0) = Y_* \tag{14a}$$

$$Y(H) = Y_H \tag{14b}$$

where Y_* is the value of the surface mass fraction of water vapor and Y_H is the value of the mass fraction of water vapor in the stratosphere. The solution of equation (13) subject to equation (14) is given by

$$Y = \frac{Y_* \sinh [\bar{\lambda}(1-\bar{z})] + Y_H \sinh [\bar{\lambda}\bar{z}]}{\sinh \bar{\lambda}} \tag{15}$$

where $\bar{z} = z/H$ and $\bar{\lambda} = H\sqrt{A_o/K_o}$. The first question that arises is, Does this model give a reasonable upward flux at surface, i.e., is the overall evaporation process modeled? The flux at the surface is given by $F_* = -K_o(dY/dz)_*$ and can be found by differentiating equation (15). The resulting expression is

$$F_* = \sqrt{A_o K_o}\,[Y_* \tanh \bar{\lambda} - Y_H/\sinh \bar{\lambda}] \tag{16}$$

A computation of F_* requires an estimation of the various parameters in the above expression. At 30°N latitude, Junge (ref. 20) estimated the average residence time of water vapor in the atmosphere to be about eight days, and the height of the troposphere is about 15 km. The value of the stratospheric mass fraction is about 2.5×10^{-6} [see Harries (ref. 21)]. A typical value of K_o used in one-dimensional calculations of the atmosphere is 10^{-5} km^2/s and thus, $\bar{\lambda} \simeq 6$. The form of boundary condition at the surface is taken from Manabe and Wetherald (ref. 8) and is given by

$$Y_* = \frac{0.622\, h_*\, e_s(T)}{p_* - h_*\, e_s(T)} \tag{17}$$

where $e_s(T)$ is the saturation vapor pressure, and h_* and p_* are the surface relative humidity and pressure, respectively. Typical values of Y_* are on the order of 10^{-2} to 10^{-3}. Under these conditions, the surface flux can be approximated by

$$F_* = \sqrt{A_o K_o}\; Y_* \tag{18}$$

When the values of A_o, K_o and Y_* are substituted into equation (18), the surface flux is found to be about 0.2×10^{-7} km/s. Existing data [Junge (ref. 20)] show $F_* \simeq 0.3 \times 10^{-7}$ km/s; thus the computed surface fluxes are considered reasonable. Figure 16 shows the results of two separate calculations using The Aerospace Corporation's one-dimensional photochemical atmospheric model along with observational data taken from Mastenbrook (ref. 14) and Oort and Rasmussen (ref. 30) interpolated for 30°N latitude. The values of the parameters are not unreasonable and have been chosen in order to show the calculated distributions of water vapor that not only bracket the observed data, but in addition yield reasonable agreement. Curve (a) corresponds to the values: $A_o = 5.8 \times 10^{-6}$ day^{-1} (two-day rainout period), $K_o = 2 \times 10^{-5}$ km^2/s, $Y_* = 0.24 \times 10^{-2}$ gm/gm-air; whereas curve (b) corresponds to $A_o = 2 \times 10^{-6}$ s^{-1} (5.8-day rainout period), $K_o = 0.66 \times 10^{-5}$ km^2/s, $Y_* = 0.69 \times 10^{-2}$ gm/gm-air. These calculations give surface fluxes of about 0.25×10^{-7} km/s. These calculations were carried out for two different chemistry models; namely, an original chemical model used by Widhopf, et al. (ref. 22) (see Table I) and that currently published by the NASA workshop (see Table II). Even though certain key hydroxyl reaction rates were changed, the results for the water vapor distributions are relatively insensitive to this change. The numerical results of the one-dimensional model were compared with equation (15) using the corresponding parameters and found to differ by less than two percent, thereby confirming the fact that the water vapor profile is mainly controlled by the transport/rainout mechanisms in the troposphere.

Extension of the one-dimensional model to two dimensions is generally straightforward. The average residence time of the water vapor as a function of latitude is taken from Junge (ref. 20). In addition, the transport due to circulation as well as both gradient and countergradient turbulent fluxes of water vapor is included.

Regarding the assumption of A_o being constant in the troposphere equal to an average value estimated from data, it should be emphasized that the model was not developed to predict the actual precipitation at each point in the troposphere (which is not known, anyway) but to simulate the total precipitation in a column at each latitude (since the data can only show total precipitation that reaches the surface). In addition, since the amount of precipitation is proportional to the amount of water vapor present, most of the precipitation occurs in the first 5-6 km, and this agrees reasonably well with observations of cloud cover.

We should also point out the lack of success in attempting to develop a water vapor model based on a relative humidity formulation. In this type of model, the relative humidity is monitored; when its value reaches a certain predetermined level, precipitation is assumed to occur. The results of this type of model did not yield a dry stratosphere as observed by Mastenbrook (ref. 14).

With a two-dimensional model of the water vapor available, a simplified coupled-radiation species and circulation model of the natural atmosphere can be put together. The description of the model of the natural atmosphere is given in the next section and includes the water-vapor distributions calculated using this model of rainout/washout.

NATURAL ATMOSPHERE

In order to assess the effects of the injection of pollutants on the chemical and thermal structure of the atmosphere, one must have knowledge of the structure of the natural atmosphere. The computation of the coupled chemical, thermal and dynamic structure of the atmosphere tends to be very expensive from a computational standpoint. To alleviate this problem, one can consider a simplified atmospheric model in which the perturbed thermal structure of the atmosphere is not coupled back to the dynamics. A consistent calculation of the perturbed structure can be performed by prescribing the natural atmosphere by a coupled solution of the species conservation and energy equations with the temperature specified. The results of such a calculation would yield the meridional circulation as well as the chemical structure of the natural atmosphere. The perturbed chemical and thermal structure of the atmosphere can then be obtained by solving the coupled species conservation and energy equations, using the computed meridional circulation of the natural atmosphere. Although there is no coupling of the chemical and thermal structure to the dynamics, the resultant temperature perturbation obtained can be considered to be an upper bound, since all the perturbed energy is converted into a temperature change, rather than allowing a portion of it to perturb the circulation. This model of the natural atmosphere is described below.

The coupled model of the natural atmosphere is a modification of The Aerospace Corporation's atmospheric model. This original model was a steady-state seasonal phenomenological photochemical model of the atmosphere in which the hydrodynamic variables (mean atmospheric density, temperature, turbulent diffusion coefficients and mean meridional winds) are specified and used to solve the system of species conservation equations for the meridional distribution of trace species. The details of this model are described in the Appendix. The modification necessary to complete the model of the natural atmosphere was to couple the method of computing the meridional circulation to the solution of the species conservation equations. The resultant coupled model was then used to calculate the chemical and dynamic structure of the natural atmosphere. The water model outlined previously was also incorporated.

To demonstrate the feasibility of such a model, the natural atmosphere was simulated for the fall season (northern hemisphere). The coupled calculation was run until a steady-state solution was achieved. Figure 17 illustrates the data taken from Gebhart, et al. (ref. 23), Sticksel (ref. 24) and London (ref. 25) for the latitudinal distribution of total ozone column for the fall season. Also shown are the results of two calculations for the natural atmosphere. Curve (a) is an initial calculation carried out using the chemical system and associated reaction rate coefficients tabulated in Table I. This is essentially the chemical system used by Widhopf, Glatt and Kramer (ref. 22) to estimate the effect on ozone due to NO_x emissions from a combined fleet of supersonic and subsonic aircraft projected to be operational in 1990. Curve (b) is the result of a similar calculation in which the important reactions involving NO_3 and

N_2O_5 have been included together with use of the latest updated reaction rates from the NASA summary (ref. 51), as shown in Table II. The effects of day/night averaging were also included in this latter calculation. The converged solution, curve (a), shows good agreement with the data in the northern hemisphere (maximum difference, about nine percent). The ozone column in the southern hemisphere (maximum difference, about 16 percent) is not in as good agreement with the available data as is the northern hemisphere calculation. The results given by curve (b) show a substantial increase in the O_3 column throughout the meridional plane [approximately a 50 percent increase from curve (a) near the northern polar region]. This result is essentially due to the change in the reaction rate for the reaction R10: $NO + HO_2 \rightarrow OH + NO_2$ from a value of 2.3×10^{-13} to 8×10^{-12}, a factor of about 35 increase. Since the major destruction of ozone through NO_x occurs by the reaction R7, $O_3 + NO \rightarrow O_2 + NO_2$, the effect of increasing R10 is to reduce the effect of R7. This result has also been observed in our one-dimensional model as well as by other investigators in both one-dimensional and two-dimensional models. Since the reaction rate R10 has been verified, it is possible that there may be other phenomena which have not been properly accounted for, either by having an incorrect reaction rate constant, not including pertinent chemical systems, or an incorrect prescription of the dynamics. However, to date, the latest set of reaction rates corresponding to curve (b) is the state-of-the-art; thus, until further refinement is made, these rates are used for current atmospheric model simulations. Due to the coupling of the diffusion coefficients to the computation of the circulation, it is beyond the scope of this work to investigate the sensitivity of the resultant ozone distribution to modifications in both the diffusion coefficients and chemical system.

Figure 18 shows the vertical distribution of ozone for various latitudes (10°N, 40°N, 60°N and 80°N) corresponding to curves (a) and (b) in figure 17. The results for solution (a) are in agreement with data [Wilcox (ref. 7), and Hering and Borden (refs. 26 through 29)], with the peaks generally being about 2 km lower than the peaks in the data. The results for solution (b) show a large increase in the ozone level throughout the meridional plane.

Figure 19 shows the resultant converged solution of water vapor profiles at 0°N, 30°N and 60°N corresponding to solution (b). Included is the corresponding data of Oort and Rasmussen (ref. 30) for the tropospheric water vapor. The calculated results are in very good agreement with the data at 0°N and 30°N, and slightly low at 60°N. However, these reduced values at 60°N are most probably associated with the lower boundary value used in the calculation. The calculation also produces a very dry stratosphere with a mass fraction of $2.5\text{-}3 \times 10^{-6}$ gm/gm-air. The water vapor results corresponding to the chemical system in Table II are essentially the same since, as pointed out previously, chemistry is a higher order effect on the water vapor profiles.

Figures 20 and 21 show the resultant converged solution for the meridional heating distribution and circulation pattern. Comparison of figure 21 and figure 5 shows the computed ozone profiles give similar type streamline patterns in the northern hemisphere as those obtained using the prescribed ozone profiles by Wilcox, et al. (ref. 7). However, the circulation pattern in the southern hemisphere has changed somewhat.

One important result has been in regard to the N_2O profiles. In the original calculation by Widhopf (ref. 4), which used the meridional circulation calculated by Louis (ref. 5), the N_2O at high altitudes was shown to be high when compared to data [Ehhalt, et al. (ref. 31), Farmer, et al. (ref. 32), Murcray, et al. (ref. 33), and Schütz, et al. (ref. 34)]. These high values were attributed to the N_2O being controlled by the meridional circulation at the high latitudes, convecting it upward and then diffusing it meridionally. In the present calculation, the computed circulation in the high latitudes produces a lower upward velocity than does that of Louis and thus lowers the value of N_2O. This can be seen in figure 22.

Thus, the coupled model developed for the natural atmosphere has been found to produce distributions of water vapor and ozone that are in reasonable agreement with data. With this fact in mind, an investigation of the effects of NO_x and HO_x pollutant injection on ozone and stratospheric temperature can be made.

PERTURBED ATMOSPHERE

The development of an atmospheric model to investigate changes in both the chemical and thermal structures of the atmosphere, arising from the injection of pollutants, involves coupling the individual species conservation equations to the energy equation. In this model, the circulation is held fixed as computed in the natural atmosphere; thus, the coupling of the temperature perturbations to the meridional circulation is not considered. Because of this lack of coupling, one can expect the calculated temperature perturbations to be an upper bound, since all the energy changes go into driving the temperature perturbation. The temperature perturbations are coupled back into the reaction rate coefficients in the computation of the chemical structure of the perturbed atmosphere. The formulation of the energy equation is described below.

The energy equation expressed in terms of the potential temperature is given by equation (19).

$$\frac{\partial \theta}{\partial t} + \frac{v}{r}\frac{\partial \theta}{\partial \phi} + w\frac{\partial \theta}{\partial z} = \dot{Q}_E + \frac{\dot{Q}_R}{\pi} \tag{19}$$

To simplify the calculation, equation (19) can be written in terms of the perturbation of potential temperature

$$\frac{\partial \theta'}{\partial t} + \frac{v}{r}\frac{\partial \theta'}{\partial \phi} + w\frac{\partial \theta'}{\partial z} = \dot{Q}'_E + \frac{\left[\dot{Q}'_R - \frac{\pi'}{\pi_o}\left(\dot{Q}_R\right)_o\right]}{\pi_o + \pi'} \tag{20}$$

where Q'_E is given by equation (3) with θ replaced by θ' and $\dot{Q}'_R$ is $\dot{Q}_R - (\dot{Q}_R)_o$. Here, the term $(\dot{Q}_R)_o$ is the resultant distribution of radiative sources and sinks obtained for the natural atmosphere, and $\dot{Q}_R$ is the total radiative heating or cooling in the perturbed atmosphere. The term $\pi'/\pi_o\,(Q_R)_o$ is, in general, smaller than Q'_R (less than one percent near the tropopause and about eight percent near 50 km) and thus can be neglected. Therefore, equation (20) can be approximated by

$$\frac{\partial\theta'}{\partial t} + \frac{v}{r}\frac{\partial\theta'}{\partial\phi} + w\frac{\partial\theta'}{\partial z} = \dot{Q}'_E + \frac{\dot{Q}'_R}{\pi_o} \tag{21}$$

Equation (21) is solved in the domain $-90^\circ \leq \phi \leq 90^\circ$ and $15 \leq z \leq 50$ km. The lower boundary of 15 km has been chosen since the radiation model developed by Ramanathan (ref. 1) is valid only in the stratosphere. The solution of the energy equation down to the surface requires the need of a very complex tropospheric radiation model, which is not available at the present time. Equation (21) requires four boundary conditions on θ'. At the poles we have prescribed $\partial\theta'/\partial\phi = 0$, whereas at the upper and lower boundaries we have prescribed $\partial\theta'/\partial z = 0$. The use of the lower boundary condition will be discussed later in this section.

The energy equation is solved using a combined leap-frog and Dufort-Frankel finite-difference scheme similar to that used for the solution of the species conservation equations. The energy equation is coupled to the species equations in the following manner: As the new mass fractions Y_i^{n+1} are computed, they are used to evaluate the radiation term in the energy equation to compute θ' at time $(n+1)\Delta t$. The maximum time step for which the calculation was found to remain stable was about one day and was used in the computation of both species and temperature perturbations. With θ' known, the actual temperature $T = \theta\pi$ is found; thus $T' = T - T_o$ (where T_o is the temperature distribution in the natural atmosphere) can be evaluated. The new temperature is then coupled back to the reaction rates for the computation of the new species mass fraction. The calculation is continued until a steady-state solution is obtained.

A discussion of the results of two separate investigations of the effects of the injection of NO_x and HO_x pollutants on the chemical and thermal structure of the atmosphere follows.

Case 1: Perturbed Atmosphere--NO_x and HO_x

Since the initiation of this study, the importance of including the effects of subsonic flying aircraft has become apparent. This is a result of the fact that the subsonic aircraft fleets were found to produce a greater amount of NO_x than the higher flying SSTs; this potentially results in an overall increase of total ozone rather than a decrease [Widhopf, et al. (ref. 22)]. Table III shows a recent estimate (upper bound) supplied by the FAA (ref. 35) regarding the NO_x emissions from a combined fleet of supersonic and subsonic aircraft projected to be operational in 1990. This table includes emissions from present subsonic type aircraft that nominally cruise at 9-11 km, advanced subsonic aircraft that cruise in the altitude range of 12.5-14.5 km, and supersonic aircraft of the Concorde-Tupolev type that nominally cruise at 18 km. The variation of NO_x emissions with both altitude and latitude is seen to be large. The major source of emissions (about 80 percent) results from the subsonic fleet and is deposited mainly between 9 and 13 km. The total amount of NO_x emissions for this estimate is 2.81×10^9 kgm/yr.

With the increased understanding of the HO_x chemical cycle, it has become apparent that the effects of HO_x injection are important in determining the chemical and thermal structure of the atmosphere. Ramanathan (ref. 1) studied the sensitivity of the stratospheric temperature to changes in water vapor using a one-dimensional radiative-equilibrium model. His results showed the necessity of including HO_x injection for correctly predicting the thermal structure of the atmosphere. Two-dimensional calculations of Rao (ref. 3) did not include these HO_x effects.

The calculations to be described considered a modification of the FAA estimate of NO_x injection rates in order to account for an increased fleet of supersonic aircraft. This amounted to an increase of NO_x injection rates above 15 km by the factor 500/142. The HO_x injection rates were obtained by multiplying the final NO_x injection rates by the ratio of their emission indices 1250/17. For the present calculation, NO_x was injected as NO_2 and HO_x as H_2O. The initial conditions used for the calculation were obtained from the results of the natural atmosphere.

The perturbed atmosphere was simulated for a period of four years after which a steady-state solution was attained. Figure 23 shows the latitudinal distribution of total ozone column change. The maximum increase in total ozone is three percent and occurs about 40°N latitude. This latitude corresponds to that for peak NO_x and HO_x injection rates. Also shown, however, is the ozone column change above 15 km. Thus, it can be seen that more than two-thirds of the total column increase occurs below 15 km. The interesting result here is the production of ozone in the stratosphere. Comparison of the present results with those obtained by Widhopf, et al. (ref. 22), where NO_x was the only pollutant injected, show a similar result in the troposphere; however, a slight reduction of ozone occurred in the stratosphere (maximum total ozone column change of 1.4 percent during the fall season).

The increase of ozone in the stratosphere in the present calculations is attributed to the injection of water vapor. Figure 24 shows the resultant distributions of H_2O at $\phi = 0^o$ and 40^oN for both natural and perturbed atmospheres. The increase in ozone above 15 km is due to the reduction in the effectiveness of the NO_x catalytic destruction cycle by H_2O. In addition, the increase of the reaction rate for $NO + HO_2 \longrightarrow OH + NO_2$ can have a large effect on the reduced effectiveness of the NO_x destruction cycle. For the pure NO_x injection case, this catalytic cycle is

$$NO_2 + O(^3P) \longrightarrow NO + O_2 \qquad R6$$

$$NO + O_3 \longrightarrow NO_2 + O_2 \qquad R7$$

However, the additional injection of H_2O forms OH and HO_2 through reactions

$$O(^1D) + H_2O) \longrightarrow OH + OH \qquad R32$$

$$O_3 + OH \longrightarrow O_2 + HO_2 \qquad R9$$

The increased concentration of HO_2 reduces NO through the reaction

$$HO_2 + NO \longrightarrow OH + NO_2 \qquad R10$$

Although O_3 is depleted through R9, the depletion of O_3 through R7 has been reduced considerably due to reduction in NO through R10. In addition, NO_2 is reduced through the reaction

$$OH + NO_2 + M \longrightarrow HNO_3 + M \qquad R12$$

which in turn reduces the NO produced by the photodissociation of NO_2, i.e.

$$NO_2 + h\nu \longrightarrow NO + O(^3P) \qquad R4$$

The net result is a decrease in the effectiveness of the catalytic destruction cycle and an increase in ozone.

In the troposphere, the effect of the combined injection of NO_x and HO_x is a production of ozone. This ozone increase is due to the increased concentration of $O(^3P)$. As pointed out by Widhopf, et al. (ref. 22) in the strict NO_x

injection case, the increase in $O(^3P)$ was initiated by the oxidation of methane by OH, which then cycled through the smog chain to produce HO_2. The HO_2 reacted with NO to produce NO_2 which then photodissociated to produce $O(^3P)$, i.e.

$$HO_2 + NO \longrightarrow OH + NO_2 \qquad R10$$

$$NO_2 + h\nu \longrightarrow NO + O(^3P) \qquad R4$$

The additional injection of HO_x increases the effectiveness of smog chain on the production of $O(^3P)$ since H_2O is converted to OH by the reaction

$$O(^1D) + H_2O \longrightarrow OH + OH \qquad R32$$

The concentration of $O(^3P)$ is also increased directly by the reaction

$$OH + OH \longrightarrow H_2O + O(^3P) \qquad R38$$

This increase in $O(^3P)$ increases the ozone level through the reaction

$$O_2 + O(^3P) + M \longrightarrow O_3 + M \qquad R5$$

Thus, the combined effect of the injection of NO_x and HO_x for these calculations is to increase ozone in both the troposphere and stratosphere. It should be pointed out that these results are based on the new reaction rate measurement for R10 which has been increased by a factor of 35 over previous recommended value (Table I). Since the mechanisms in both stratosphere and troposphere are strongly dependent on the reaction $HO_2 + NO \longrightarrow OH + NO_2$, and have resulted in a substantial increase in the ozone columns in the natural atmosphere above observed levels, one should not draw any immediate definite conclusions in regard to the magnitude of the production of ozone for this NO_x and HO_x pollution case. The increased ozone levels in the natural atmosphere are particularly disturbing, and it is possible that other reaction rates involving the hydroxyls are still inaccurate and could influence the present results. This is an important area of future investigation, and possible candidates are hydroxyl reactions involving production or depletion of $O(^3P)$ and those depleting ozone.

Figure 25 shows the corresponding resultant steady-state meridional distribution of temperature perturbation (T') in ^oK. The results exhibit two interesting features. First, the contours of T' are shown to be nearly symmetrically centered around the equator in the region 40^oS to 40^oN between

15 and 25 km. Second, the maximum temperature perturbation, which is approximately 5.9°K, is located at the lower boundary near the equator. However, the temperature perturbation is less than one degree above 19 km. In order to gain some understanding of the resultant perturbations, we must examine the physical mechanisms that produce these perturbations.

Since the complete energy equation is solved in this investigation, the steady-state distribution of T' is achieved by a balance of convection, diffusion and radiation of perturbed energy. The perturbations are initially generated through the radiation term by a perturbation in water vapor and ozone after which the convection and diffusion come into play by redistributing the perturbed energy. Since the time scales for transport are much longer than those for the chemistry changes, the perturbed atmosphere must be simulated for a number of years before a steady-state condition is attained.

From an analysis of the steady-state solution, it was determined that the heating due to radiation (Q'_R) in the equatorial region near the lower boundary is produced by the 9.6μ O_3 band due to the increase in ozone concentration. In addition, heating due to the 15μ CO_2 band occurs because of the increased amount of water vapor aloft which reduces the cooling by CO_2 through the H_2O overlap region. At higher altitudes, the atmosphere is cooled by the increased water vapor through the H_2O emission band. The peak cooling is less than -0.5°K. In the equatorial region aloft, there exists a region of positive temperature perturbation which is due to the vertical diffusion of perturbed energy from the lower regions. The nearly symmetric contours of T' in the equatorial region are a result of the closed circulation cell (see fig. 21) which redistributes the perturbed energy in the region 15 to 25 km.

Since the maximum temperature perturbation occurs at the lower boundary and is of substantial magnitude, it is important to investigate the effect of the lower boundary condition on the resultant perturbations. For this study, a one-dimensional version of the two-dimensional model was used. In this case, the energy equation [eq. (21)] reduces to

$$\frac{\partial \theta'}{\partial t} = \frac{\partial}{\partial z}\left(K_{zz}\frac{\partial \theta}{\partial z}\right) + \frac{Q'_R}{\pi_o} \tag{22}$$

Under steady-state conditions

$$\frac{\partial}{\partial z}\left(K_{zz}\frac{\partial \theta'}{\partial z}\right) + \frac{Q'_R}{\pi_o} = 0 \tag{23}$$

As might have been expected, equation (23) requires the total vertical flux of perturbed energy to be constant, i.e.

$$F'_e + F'_R = \text{constant} \tag{24}$$

where $F'_e = -K_{zz}(\partial\theta'/\partial z)$ and $F'_R = -\int (Q'_R/\pi_o)\,dz$. We consider two different boundary conditions for this investigation. The first condition, $\partial\theta'/\partial z = 0$, is identical to the boundary condition used in the two-dimensional calculation, and the second is $T' = 0$ at the lower boundary. The second boundary condition is physically unrealistic for the present injection case since the major portion of the injection is below 15 km. However, some physical insight can be gained by using such a boundary condition.

Figure 26 shows the resultant one-dimensional distribution of temperature perturbation for both boundary conditions, i.e., (a) $\partial\theta'/\partial z = 0$ and (b) $T' = 0$. For these calculations, we have used the injection rates at 30°N latitude. Use of the boundary condition $\partial\theta'/\partial z = 0$ results in a vertical temperature distribution similar to that obtained in the two-dimensional calculation, with the peak temperature perturbation occurring at the boundary with a value of approximately 0.5°K and the crossover point from positive to negative perturbations occurring at about 21 km. For the two-dimensional result (fig. 25) at 30°N latitude, the peak value of T' is approximately 1°K and occurs at the lower boundary with the crossover occurring at 20 km. Due to the large latitudinal gradient in T' calculated in the two-dimensional results, it is not unrealistic that the one-dimensional calculations predict T' to be about one-half that obtained with the two-dimensional calculations.

Use of the second boundary condition $T' = 0$ results in a much lower positive temperature perturbation ($T' \approx 0.08$°K) and is found to occur 1 km above the boundary. Above 25 km, these results show less cooling than in the $\partial\theta'/\partial z = 0$ case; however, below 25 km, there is more cooling (or less heating) for the $T' = 0$ case. These results are consistent since the $T' = 0$ case allows a finite transfer of energy downward at the lower boundary, thus allowing for an energy removal mechanism which did not exist for the case $\partial\theta'/\partial z = 0$.

Since the results exhibit the strong sensitivity of the temperature perturbation to the lower boundary condition, the resultant maximum temperature perturbation of 5.9°K for the two-dimensional calculations would appear to be on the high side. In addition, as pointed out earlier, since the temperature perturbations are not coupled back to the dynamics, one should also expect the magnitude of the calculated temperature perturbation to be on the high side. However, it is not clear at this time what the appropriate lower boundary condition should be. It is evident, at this time, that the only logical method of alleviating the problem of the lower boundary condition is to solve the energy equation down to the surface and prescribe $T' = 0$ at this point. This method requires the use of a complex tropospheric radiation model, which is not available at this time, but which should be developed.

Case 2: Perturbed Atmosphere--H_2O

In recent years, there has been considerable interest in the development of new types of propulsion systems for high-flying aircraft. Prior to implementation of these systems, it is important to determine whether any detrimental effects to the atmosphere will arise from their use. In particular, the use of liquid hydrogen has been under consideration as a new type of fuel for these high-flying aircraft. Since the exhaust emissions from this type of system contain HO_x, and with the recent knowledge of the increased relative importance of HO_x chemistry on the ozone layer, it is important to investigate this potential problem area.

The hypothetical fleet used in this study consists of 200 liquid hydrogen-fueled aircraft flying six hours per day at an altitude of 20.6 km through the latitudinal corridor 35°N-55°N. The exhaust emissions were specified to be in the form of water vapor at a rate of 28.5 kgm/s. These emissions were uniformly distributed through the corridor 35°N-55°N and between 20 and 21 km. Starting with the natural atmosphere as the initial condition, the perturbed atmosphere was simulated for a period of two and one-half years after which a steady-state solution was essentially attained. For this calculation, the chemical system used was that shown in Table I as modified by Table II. The meridional circulation was taken from the results of the natural atmosphere (fig. 21).

Figure 27 shows the resultant meridional distribution of percent change in ozone column. The peak change in the northern hemisphere is about 0.16 percent increase, and occurs at 50°N, whereas in the southern hemisphere the change is about 0.28 percent increase and occurs at 70°S. In the equatorial region (40°S-20°N), a 0.12 percent decrease in ozone has occurred. Also shown is the column change above 15 km. Note that there is a decrease in ozone below 15 km except in the equatorial region where no change is observed. The mechanism for ozone increase in the stratosphere with regard to HO_x injection has been discussed in the previous section. The decrease in ozone below 15 km (and up to 25 km in the equatorial region) is due to the reduction in $O(^3P)$ by HO_2 as well as by the depletion of O_3 by OH, i.e.

$$HO_2 + O(^3P) \longrightarrow OH + O_2 \qquad \text{R15}$$

$$O_2 + O(^3P) + M \longrightarrow O_3 + M \qquad \text{R5}$$

$$O_3 + OH \longrightarrow O_2 + HO_2 \,. \qquad \text{R9}$$

Figure 28 shows the resultant water vapor profiles at 0°N and 40°N. In the region of injection, the water vapor concentration has increased by about 25 percent. The changes in total ozone column in the southern hemisphere are due to the water vapor being convected and diffused southward (see fig. 21).

Figure 29 shows the resultant meridional distribution of temperature-perturbation in °K. The maximum positive temperature perturbation of 0.7°K occurs at the lower boundary near the equator. The peak negative perturbation is -0.7°K and occurs near the northern polar region at about 21 km. Note the nearly symmetrical contours centered around the equator below 20 km. This result is similar to that found in the NO_x and HO_x injection, although not as wide and with a much lower zero contour. The cooling is initiated through the radiation term in the energy equation by the increased water vapor concentration after which convection and diffusion come into play in redistributing the energy. The heating in the equatorial region is due to the increased concentration of ozone as well as the increase in water vapor aloft which reduces the cooling of the 15μ CO_2 band through the H_2O transmissivity factor. Convection and diffusion then again become important in redistributing this energy.

The physical aspect of the lower boundary condition with regard to the resulting temperature perturbations has already been discussed, and it should be emphasized that it also applies here. However, based on these results, it appears that the present hypothetical fleet of liquid hydrogen-fueled aircraft has a minimal effect on both the thermal and chemical structure of the atmosphere.

CONCLUSIONS

This study was initiated to provide the ability of including active HO_x perturbations in stratospheric pollution studies and to investigate any resulting stratospheric temperature changes. The primary results of this investigation are:

(1) The Ramanathan radiation model provides a very good description of the meridional stratospheric heating and cooling rates, provided the solar radiation is calculated using a diurnal averaging technique.

(2) The computation of the meridional circulation using the energy and continuity equations (given the temperature distribution) has been found to be sensitive to the prescription of both turbulent diffusion coefficients as well as the radiation model. Due to the requirement of satisfying an integral constraint on the vertical velocity when using this approximate technique, the resultant circulations are, in general, not unique.

(3) The resultant seasonal meridional circulation patterns computed using the approximate method have been used to study the dispersion of inert tracers (carbon-14 and tungsten-185). The results of this study have shown the adequacy of these computed circulation patterns in describing the decay of these inert tracers.

(4) An active water vapor model was developed which is simple in concept and yields two-dimensional steady-state water vapor distributions that are in agreement with available tropospheric measurements. The model also yields a dry stratosphere in agreement with available data. In addition, the calculated precipitation is in relatively good agreement with measurements, being approximately 75 percent high in the region 0-30° latitude and within 25 percent of the measurements at higher latitudes.

(5) The inclusion of the latest chemical reaction rates has been found to produce more ozone (approximately 25 percent) in the natural atmosphere than has been previously calculated and/or measured. This result indicates the possibility that other chemical species are important, although presently not included, or that certain reaction rates are still uncertain, in particular those involving the hydroxyls.

(6) A coupled species-radiation model was developed to study active NO_x and HO_x pollutant problems. It has been found herein that transport is very important in determining the distribution of the temperature perturbation in the stratosphere. Thus, one-dimensional calculations may be limited in this regard.

(7) At the initiation of this study the pollution emitted by high flying supersonic aircraft was to be investigated. However, subsequent work by Hidalgo and Crutzen (ref. 52) and Widhopf, et al. (ref. 22) indicates that the emissions by subsonic aircraft flying in the troposphere are important in the overall evaluation of the effect of aircraft emissions on atmospheric ozone. In this regard, the effect of NO_x and HO_x emissions from a modified FAA projected fleet of both supersonic and subsonic aircraft was investigated and found to produce a maximum total ozone column increase of three percent located at 40°N latitude. In addition, the maximum calculated temperature perturbation was 6°K and occurred at the lower boundary (15 km) near the equator. It should be emphasized that these results were obtained using the newly measured higher rate for the HO_2 + NO reaction which yields approximately a 25 percent overprediction of the total ozone column--in the natural atmosphere [see item (5)]. The necessity of choosing the lower boundary at 15 km was due to the fact that the Ramanathan radiation model is only valid in the stratosphere. For this case, in which 80 percent of the NO_x and HO_x has been injected in the troposphere, the correct lower boundary condition for the temperature perturbation is uncertain. From a sensitivity study performed using a one-dimensional version of the two-dimensional model, the resultant temperature perturbations have been found to be sensitive to the lower boundary condition, and it would appear that the present boundary condition used in the two-dimensional model has overestimated the temperature perturbation. In addition, the method of computing the temperature perturbation by decoupling the circulation from the calculation would also lead to an overprediction in the results. Thus, the 6°K perturbation is considered an overestimation of the actual effect. It has become apparent that the inclusion of a tropospheric radiation model is a necessity in order to accurately determine the temperature perturbation, especially in the case of subsonic injections. Such a model is not available but should be developed in the near future.

(8) The effect of stratospheric HO_x emissions by a hypothetical fleet of 200 liquid hydrogen-fueled aircraft cruising at 20.6 km was found to be minimal with regard to both temperature and ozone (less than 0.25 percent increase in ozone and a maximum temperature perturbation of 0.7°K).

APPENDIX

Basic Atmospheric Model

The model is a phenomenological photochemical model of the atmosphere in which the hydrodynamic variables (mean atmospheric density, temperature, turbulent diffusion coefficients, and mean meridional winds) are either specified from observations or obtained indirectly from observations as a function of time during the year and used to solve the system of species conservation equations for the meridional distribution of trace species throughout the year. The original formulation of the model, discussed in Widhopf and Taylor (ref. 36) and Widhopf (ref. 4), is basically designed to examine relatively small changes in the ozone concentration as a function of the time of year throughout the meridional plane, since any resultant changes in the species concentration occurring as a result of the introduction of a pollutant are not coupled back to the atmospheric dynamics or temperature distributions.

The governing species conservation equation is derived following the general procedure outlined by Reed and German (ref. 11) for representing the turbulent transport flux due to large-scale eddies. In the meridional plane this equation, written in terms of the mass mixing ratio, is of the form

$$\frac{\partial \rho Y_i}{\partial t} + \frac{\partial \rho w Y_i}{\partial z} + \frac{1}{\cos\phi}\frac{\partial \rho v Y_i \cos\phi}{r\partial\phi} = \frac{\partial}{r\partial\phi}\left\{\rho k_{\phi z}\frac{\partial Y_i}{\partial z} + \rho k_{\phi\phi}\frac{\partial Y_i}{r\partial\phi}\right\}$$
$$+ \frac{\rho}{r}\left\{(2k_{zz} - k_{\phi z}\tan\phi)\frac{\partial Y_i}{\partial z} + (2k_{z\phi} - k_{\phi\phi}\tan\phi)\frac{\partial Y_i}{r\partial\phi}\right\}$$
$$+ \frac{\partial}{\partial z}\left\{\rho k_{zz}\frac{\partial Y_i}{\partial z} + \rho k_{\phi z}\frac{\partial Y_i}{r\partial\phi}\right\} + \omega_i + S_1 \qquad i=1,2,\ldots \qquad \text{(A1)}$$

where Y_i is the mass mixing ratio ρ_i/ρ of the i^{th} chemical species, ρ is the local mean atmospheric density, t is the temporal variable, $r = z + R_e$ (where R_e is the mean radius of the earth and z is the altitude measured from and normal to the earth's surface), ϕ is the latitude, ω_i is the photochemical rate of production/depletion of the i^{th} species, and S_i is the local source/sink effect. The components of the tensor $k_{\alpha\beta}$ represent the diffusion coefficient in the respective directions arising from large-scale eddy motions, while v and w are the components of the mean circulation in the meridional and vertical directions, respectively. This equation is solved for each of the trace species considered.

Chemical Model

The chemical system considered in this investigation includes the following species: $O(^1D)$, $O(^3P)$, O_2, O_3, NO, N_2O, NO_2, OH, H_2O, HO_2, H_2O_2, HNO_3, N, H, N_2, CO, CH_4, NO_3 and N_2O_5. Smog-type reactions initiated by the oxidation of methane by OH, which may be important in the lower regions of the atmosphere, are also included [Crutzen (ref. 37)]. These reactions also include the species CH_3, CHO, CH_2O, CH_3O, CH_3O_2 and CH_3O_2H. The specific reaction system and the associated reaction-rate coefficients used in this investigation are tabulated in Tables I and II. This chemical system is based essentially on that recommended by the NASA-CFM Report.

Computation of the absorption of solar radiation is an integral step in determining the chemical structure of the atmosphere, since many of the important reactions in the atmosphere are photochemical processes. Using the solar flux data compiled by Ackerman (ref. 38), the diurnally averaged local photodissociation rates J_i are calculated at every location in the atmosphere at each time step by a technique developed by Kramer and Widhopf (ref. 39). The time variation of the solar zenith angle with latitude and solar declination is included in the determination of J_i. The absorption cross sections utilized to compute J_i for the various species are outlined in Widhopf (ref. 4).

The effect of chlorine in the atmosphere was not included in this investigation. From NAS studies (ref. 40), the inclusion of chlorine should attenuate the effect of NO_x destruction of ozone due to the formation of $ClONO_2$.

Boundary Conditions

The computational domain considered in this investigation extends from the north to the south pole, with a ten-degree meridional resolution; and from the surface to 50 kilometers, with a vertical resolution of $\Delta z = 1$ km from the surface to 35 kilometers, and $\Delta z = 2.5$ km up to the upper boundary. At the polar regions, a zero latitudinal flux is assumed.

A fixed ozone concentration [$6(10)^{11}$ molecules/cc] was imposed at the lower boundary, as interpreted from the meridional distributions compiled by Dütsch (ref. 41) and Hering and Borden (refs. 26-29) [as summarized in the data compilation of Wu (ref. 42)]. The concentration of N_2O at the lower boundary was prescribed as an average value (0.481 ppmm) interpreted from the tropospheric measurements of Schutz, et al. (ref. 34), and Goldman, et al. (ref. 43). The latitudinal variation of the mass mixing ratio of CO at the surface was interpreted from the measurements of Seiler (ref. 44). The mass mixing ratio of CH_4 (0.75 ppmm) at the lower boundary was specified from the measurements of Ehhalt, et al. (ref. 31). Injection of NO and NO_2 resulting from the anthrophotogenic activities were specified at the lower boundary as interpreted from the estimates of Robbins and Robinson (ref. 45).

The species $O(^3P)$, $O(^1D)$, OH, HO_2, N and H were taken to be in photochemical equilibrium at the lower boundary because of their relatively short lifetimes, while HNO_3, NO_2, NO and H_2O_2 were removed from the troposphere by simulating atmospheric rainout/washout. HNO_3 was removed at the average rates defined by Junge (ref. 46), while NO_2, NO and H_2O_2 were assumed to be removed at one-tenth this rate.

The species $O(^3P)$, $O(^1D)$, O_3, OH, HO_2, H_2O_2, N and H were assumed to be in photochemical equilibrium at the upper boundary, while the mass mixing ratios of NO_2, N_2O, CH_4, CO and HNO_3 were analytically continued to the upper boundary by a second-order extrapolation in space and time described by Widhopf (ref. 4) and Widhopf and Taylor (ref. 36). This extrapolation allows the use of centered spatial differencing at this boundary, while also eliminating the necessity of specifying a boundary condition for these species at this location. It is an accurate and stable method of evaluating conditions at computational boundaries [Victoria and Widhopf (ref. 47)] when the physical mechanisms interior to the computational domain govern the boundary value. This is the case for N_2O, NO_2, CH_4, CO and HNO_3 which are being transported up into the higher regions of the stratosphere.

Transport Data

The meridional distributions of both the mean density and temperature were specified using the data obtained from ten years of observations which were analyzed and compiled by Louis (ref. 5). These averaged data are specified from the surface to 68 km for the entire meridional plane and for each of the four seasons.

Luther (ref. 12) has analyzed the heat transfer, temperature and wind variance data of Oort and Rasmussen (ref. 30) using the procedure outlined by Reed and German (ref. 11) for defining the components of the anisotropic turbulent eddy diffusivity tensor. The three components ($k_{\phi\phi}$, $k_{\phi z}$ and k_{zz}) are specified for the northern hemisphere from the surface to 60 km. Values for the components of the diffusivity tensor in regions where observational data were not available were obtained by Luther by extrapolation, using the results of Hunten (ref. 48) and Newell, et al. (ref. 49). These coefficients are specified for each month and were initially used to parameterize the components of the turbulent diffusivity tensor. The values for the southern hemisphere were obtained by reflecting the northern hemispheric values, shifted by six months, and applying them appropriately in the southern hemisphere. However, in testing these transport coefficients against the dispersion of inert tracers in the atmosphere, they were found not to be totally adequate [Widhopf (ref. 4)] and were improved by numerical experimentation. The results are described by Widhopf, et al. (ref. 22).

Numerical Scheme

An accurate (second order in space and time) time-dependent numerical finite difference scheme developed by Widhopf and Victoria (ref. 50), which is explicit in space and implicit in time and efficiently overcomes the "stiff" nature of the chemical system, is used to solve the governing individual species conservation equations. Details of the scheme as applied to this problem are discussed in Widhopf (ref. 4) and Widhopf and Taylor (ref. 36).

REFERENCES

1. Ramanathan, V.: Simplified Stratospheric Radiative Transfer Model: Theoretical Estimates of the Thermal Structure of the Basic and Perturbed Stratosphere. Presented at the Second International Conference on Environmental Impact of Aerospace Operations in the High Stratosphere, AMS/AIAA (San Diego, CA), July 1974.

2. Rao, V.R.K.: Numerical Experiments on the Steady-State Meridional Structure and Ozone Distribution in the Stratosphere. Mon. Wea. Rev., vol. 101, 1973, pp. 510-527.

3. Rao, V.R.K.: The Steady-State Structure of the Natural Stratosphere and Ozone Distribution in a 2-D Model Incorporating Radiation and O-H-N Photochemistry and the Effects of Stratospheric Pollutants. Atmosphere, vol. 14, no. 3, 1976, pp. 214-236.

4. Widhopf, G.F.: A Two-Dimensional Photochemical Model of the Stratosphere Including Initial Results of Inert Tracer Studies. Proceedings of the Fourth Conference on CIAP, T.M. Hard and A.J. Broderick, eds., Dept. of Transportation, DOT-TSC-OST-75-38, Feb. 1975, pp. 376-389.

5. Louis, J.F.: A Two-Dimensional Transport Model of the Atmosphere. Ph.D. Dissertation, University of Colorado, 1975.

6. Dopplick, T.G.: Radiative Heating of the Global Atmosphere. J. Atmos. Sci., vol. 29, 1972, pp. 1278-1294.

7. Wilcox, R.W., Nastrom, G.D., and Belmont, A.D.: Periodic Analysis of Total Ozone and its Vertical Distribution. CDC Rept. 3 (CR-137737), 1975, p. 24.

8. Manabe, S., and Wetherald, R.T.: Thermal Equilibrium of the Atmosphere with a Given Distribution of Relative Humidity. J. Atmos. Sci., vol. 24, 1967, pp. 241-259.

9. Murgatroyd, R.J., and Singleton, F.: Possible Meridional Circulations in the Stratosphere and Mesosphere. Quart. J. Roy. Meteorol. Soc., vol. 87, 1961, pp. 125-135.

10. Vincent, D.G.: Mean Meridional Circulations in the Northern Hemisphere Lower Stratosphere During 1964 and 1965. Quart. J. Roy. Meteorol. Soc., vol. 94, 1968, pp. 333-349.

11. Reed, R.J., and German, K.E.: A Contribution to the Problem of Stratospheric Diffusion by Large-Scale Mixing. Mon. Wea. Rev., vol. 93, 1965, pp. 313-321.

12. Luther, F.M.: Monthly Values of Eddy Diffusion Coefficients in the Lower Stratosphere. Preprint 73-498, AIAA (Denver, CO), July 1973.

13. Glatt, L., and Widhopf, G.F.: Improved Two-Dimensional Time-Dependent Transport Coefficients using Distributions of Nuclear Debris in the Atmosphere. EOS Trans., vol. 57, Apr. 1976, p. 300.

14. Mastenbrook, H.J.: The Variability of Water Vapor in the Stratosphere. J. Atmos. Sci., vol. 28, 1971, pp. 1495-1501.

15. Newell, R.E., Vincent, D.G., and Kidson, J.W.: Interhemispheric Mass Exchange from Meteorological and Trace Substance Observation. Tellus, vol. 21, no. 5, 1969, pp. 641-647.

16. Telegadas, K.: The Seasonal Stratospheric Distribution and Inventories of Excess Carbon-14 from March 1955 to July 1969. U.S. Atomic Energy Commission, Health and Safety Lab., Report No. 243, 1971, pp. 3-86.

17. Johnston, H.S., Kattenhorn, D., and Whitten, G.: Use of Excess Carbon-14 Data to Calibrate Models of Stratospheric Ozone Depletion by Supersonic Transports. J. Geophys. Res., vol. 81, 1976, pp. 368-380.

18. Friend, J.P., Feely, H.W., Krey, P.W., Spar, J., and Walton, W.: Discussion on HASP Results. Defense Atomic Support Agency, DADA 1300, vol. 3 (Washington, D.C.), 1961.

19. Gudiksen, P.H., Fairhall, A.W., and Reed, R.J.: Role of Mean Meridional Circulation and Eddy Diffusion in the Transport of Trace Substances in the Lower Stratosphere. J. Geophys. Res., vol. 73, 1969, p. 1729.

20. Junge, C.E.: Air Chemistry and Radioactivity. Academic Press, New York and London, 1963, p. 10.

21. Harries, J.E.: The Distribution of Water Vapor in the Stratosphere. Rev. of Geophysics and Space Sciences, vol. 14, no. 4, 1976, pp. 565-575.

22. Widhopf, G.F., Glatt, L., and Kramer, R.F.: Results of a Phenomenological Time-Dependent Two-Dimensional Photochemical Model of the Atmosphere. AIAA Journal, vol. 15, 1977, p. 1322.

23. Gebhart, R., Bojkov, R., and London, J.: A Comparison of Observed and Computer Models. Beitrage zur Physik der Atmosphäre, vol. 43, 1970, pp. 209-227.

24. Sticksel, P.R.: The Annual Variation of Total Ozone in the Southern Hemisphere. Mon. Wea. Rev., vol. 98, 1970, pp. 787-788.

25. London, J.: The Distribution of Total Ozone in the Northern Hemisphere. Beitrage zur Physik der Atmosphäre, vol. 26, 1963, pp. 254-263.

26. Hering, W.S.: Ozonesonde Observations over North America, 1. Research Report AFCRL-64-30(I), Air Force Cambridge Research Laboratories, Bedford, MA, 1964.

27. Hering, W.S., and Borden, T.R., Jr.: Ozonesonde Observations over North America, 2. Environmental Research Papers no. 38, AFCRL-64-30(II), 1964.

28. Hering, W.S., and Borden, T.R., Jr.: Ozonesonde Observations over North America, 3. Environmental Research Papers no. 133, AFCRL-64-30(III), 1965.

29. Hering, W.S., and Borden, T.R., Jr.: Ozonesonde Observations over North America, 4. Environmental Research Papers no. 279, AFCRL-64-30(IV), 1967.

30. Oort, A.H., and Rasmussen, E.M.: Atmospheric Circulation Statistics. National Oceanic and Atmospheric Administration, NOAA prof. paper 5, 1971.

31. Ehhalt, D.H., Heidt, L.E., Lueb, R.H., and Roper, N.: Vertical Profiles of CH_4, H_2, CO, N_2O and CO_2 in the Stratosphere. Proceedings of the Third Conference on CIAP, A.J. Broderick and T.M. Hard, eds., Dept. of Transportation, DOT-TSC-OST-74-15, Feb. 1974, pp. 153-160.

32. Farmer, C.B., Raper, O.F., Toth, R.A., and Shindler, R.A.: Recent Results in Aircraft Infrared Observations of the Stratosphere. Proceedings of the Third Conference on CIAP, T.M. Hard and A.J. Broderick, eds., 1974, pp. 234-245.

33. Murcray, D.G., Goldman, A., Murcray, F.H., Williams, W.J., Brooks, J.N., and Barker, D.B.: Vertical Distribution of Minor Atmospheric Constituents as Derived from Airborne Measurements of Atmospheric Emission and Absorption Spectra. Proceedings of the Second Conference on CIAP, A.J. Broderick, ed., 1973, pp. 86-98.

34. Schütz, K., Junge, C., Beck, R., and Albrecht, B.: Studies of Atmospheric N_2O. J. Geophys. Res., vol. 75, 1970, pp. 2230-2246.

35. Oliver, R.C., Bauer, E., Hidalgo, H., Garner, K.A., and Wasylklwskyj, W.: Aircraft Emissions: Potential Effects on Ozone and Climate, A Review and Progress Report. Dept. of Transportation, Report No. FAA-EQ-77-3, 1977, p. 404.

36. Widhopf, G.F., and Taylor, T.D.: Numerical Experiments on Stratospheric Meridional Ozone Distributions Using a Parameterized Two-Dimensional Model. Proceedings of the Third Conference on CIAP, A.J. Broderick and T.M. Hard, eds., Dept. of Transportation, DOT-TSC-OST-73-4, Feb. 1974, pp. 376-389.

37. Crutzen, P.J.: A Discussion of the Chemistry and Some Minor Constituents in the Stratosphere and Troposphere. Pure and Applied Geophysics, vols. 106-108, 1973, pp. 1385-1399.

38. Ackerman, M.: Ultraviolet Solar Radiation Related to Mesospheric Processes. Mesospheric Model and Related Experiments, G. Fiocco, ed., Springer-Verlag, New York, 1971, pp. 149-159.

39. Kramer, R., and Widhopf, G.F.: Evaluation Daylight or Diurnally Averaged Photolytic Rate Coefficients in Atmospheric Photochemical Models. To appear in J. Atmos. Sciences, Sept. 1978.

40. Halocarbons: Effect on Stratospheric Ozone. National Academy of Sciences, 1976.

41. Dütsch, H.A.: Photochemistry of Atmospheric Ozone. Advances in Geophysics, vol. 15, H.E. Landsberg and J. Van Meighem, eds., Academic Press, New York, 1971, pp. 219-322.

42. Wu, M.F.: Observations and Analysis of Trace Constituents in the Stratosphere. Environmental Research and Technology, Inc., Annual Report, Contract DoT-OS-20217, 1973.

43. Goldman, A., Murcray, D.G., Murcray, F.H., and Williams, W.T.: Balloon-Borne Infrared Measurements of the Vertical Distributions of N_2O in the Atmosphere. Journal of the Optical Society of America, vol. 63, July 1973.

44. Seiler, W.: The Cycle of Atmospheric CO. Tellus, vol. 26, nos. 1, 2, 1974, pp. 116-135.

45. Robbins, R.G., and Robinson, E.: Sources, Abundance and Fate of Gaseous Atmospheric Pollutants. American Petroleum Inst., (Washington, D.C.), 1971.

46. Junge, C.E.: Air Chemistry and Radioactivity. Academic Press, New York and London, 1963, p. 10.

47. Victoria, K.J., and Widhopf, G.F.: Numerical Solution of the Unsteady Navier-Stokes Equations in Curvilinear Coordinates: The Hypersonic Blunt Body Merged Layer Problem. Third International Conference on Numerical Methods in Fluid Mechanics, University of Paris-Orsay, Lecture Notes in Physics, vol. II, no. 19, Springer-Verlag, Berlin, 1972.

48. Hunten, D.M.: The Philosophy of One-Dimensional Modeling. Proceedings of the Fourth Conference on CIAP, T.M. Hard and A.J. Broderick, eds. Dept. of Transportation, DOT-TSC-OST-75-38, Feb. 1975, pp. 147-155.

49. Newell, R.E., Wallace, J.M., and Mahoney, J.R.: The General Circulation of the Atmosphere and Its Effects on the Movement of Trace Substances, Part 2. Tellus, vol. 18, nos. 2,3, 1966, pp. 363-380.

50. Widhopf, G.F., and Victoria, K.J.: On the Solution of the Unsteady Navier-Stokes Equations Including Multicomponent Finite Rate Chemistry. Computers and Fluids, vol. 1, 1973, pp. 159-184.

51. Chlorofluoromethane and the Stratosphere. R.D. Hudson, ed., NASA Reference Publication 1010, NASA Goddard Space Flight Center, Greenbelt, Maryland.

52. Hidalgo, H. and Crutzen, P.J.: The Tropospheric and Stratospheric Composition Perturbed by NO_x Emissions of High Altitude Aircraft. J. Geophys. Res., vol. 82, 1977, pp. 5833-5866.

TABLE I. - BASIC CHEMICAL SYSTEM AND ASSOCIATED REACTION RATES

	REACTION	RATE COEFFICIENT[a]
1.	$O(^3P) + O_3 \rightarrow 2O_2$	$1.9(10)^{-11} \exp[-2300/T]$
2.	$O_2 + h\nu \rightarrow 2O(^3P)$	J_2
3.	$O_3 + h\nu \rightarrow O(^3P) + O_2$	J_3
4.	$NO_2 + h\nu \rightarrow O(^3P) + NO$	J_4
5.	$O(^3P) + O_2 + M \rightarrow O_3 + M$	$1.07(10)^{-34} \exp[510/T]$
6.	$O(^3P) + NO_2 \rightarrow O_2 + NO$	$9.1(10)^{-12}$
7.	$O_3 + NO \rightarrow O_2 + NO_2$	$9(10)^{-13} \exp[-1200/T]$
8.	$O_3 + NO_2 \rightarrow O_2 + NO_3$ $\lvert NO_3 + h\nu \rightarrow 2/3[NO_2 + O(^3P)] + 1/3[NO + O_2] \rvert$	$1.23(10)^{-13} \exp[-2470/T]$
9.	$O_3 + OH \rightarrow O_2 + HO_2$	$1.6(10)^{-12} \exp[-1000/T]$
10.	$NO + HO_2 \rightarrow OH + NO_2$	$2.3(10)^{-13}$
11.	$O(^3P) + H_2O \rightarrow OH + OH$	0.0
12.	$OH + NO_2 + M \rightarrow HNO_3 + M$	$\frac{2.76(10)^{-13} \exp[880/T]}{1.166(10)^{18} \exp[220/T] + [M]}$
13.	$HNO_3 + h\nu \rightarrow OH + NO_2$	J_{13}
14.	$HO_2 + O_3 \rightarrow OH + O_2 + O_2$	$1(10)^{-13} \exp[-1250/T]$
15.	$HO_2 + O(^3P) \rightarrow OH + O_2$	$3(10)^{-11}$
16.	$OH + HO_2 \rightarrow H_2O + O_2$	$2(10)^{-11}$
17.	$OH + HNO_3 \rightarrow H_2O + NO_3$ $\lvert NO_3 + h\nu \rightarrow 2/3[NO_2 + O(^3P)] + 1/3[NO + O_2] \rvert$	$8.9(10)^{-14}$
18.	$H_2O_2 + h\nu \rightarrow OH + OH$	J_{18}
19.	$H_2O_2 + OH \rightarrow H_2O + HO_2$	$1.7(10)^{-11} \exp[-910/T]$
20.	$HO_2 + HO_2 \rightarrow H_2O_2 + O_2$	$1.7(10)^{-11} \exp[-500/T]$
21.	$O_3 + h\nu \rightarrow O_2 + O(^1D)$	J_{21}
22.	$O(^1D) + M \rightarrow M + O(^3P)$	$2.2(10)^{-11} \exp[92/T]$
23.	$N_2O + h\nu \rightarrow N_2 + O(^1D)$	J_{23}
24.	$N_2O + O(^1D) \rightarrow N_2 + O_2$	$5.7(10)^{-11}$
25.	$N_2O + O(^1D) \rightarrow NO + NO$	$5.7(10)^{-11}$
26.	$NO + h\nu \rightarrow N + O(^3P)$	J_{26}
27.	$N + O_2 \rightarrow NO + O(^3P)$	$1.02(10)^{-14} T \exp[-3130/T]$
28.	$N + NO \rightarrow N_2 + O(^3P)$	$2.7(10)^{-11}$
29.	$N + NO_2 \rightarrow NO + NO$	0.0
30.	$N_2 + O(^1D) + M \rightarrow N_2O + M$	$2.8(10)^{-36}$
31.	$NO_2 + N \rightarrow N_2O + O(^3P)$	$1.4(10)^{-12}$
32.	$O(^1D) + H_2O \rightarrow OH + OH$	$2.32(10)^{-10}$
33.	$O(^1D) + CH_4 \rightarrow OH + CH_3$	$1.38(10)^{-10}$
34.	$OH + O(^3P) \rightarrow O_2 + H$	$4.2(10)^{-11}$
35.	$H + O_2 + M \rightarrow HO_2 + M$	$2.08(10)^{-32} \exp[290/T]$
36.	$H + O_3 \rightarrow OH + O_2$	$1.23(10)^{-10} \exp[-562/T]$
37.	$NO + O(^3P) + M \rightarrow NO_2 + M$	$3.96(10)^{-33} \exp[940/T]$
38.	$OH + OH \rightarrow H_2O + O(^3P)$	$1(10)^{-11} \exp[-550/T]$
39.	$N + O_3 \rightarrow NO + O_2$	$5.7(10)^{-13}$
40.	$HO_2 + h\nu \rightarrow OH + O(^3P)$	J_{40}
41.	$OH + CH_4 \rightarrow H_2O + CH_3$	$2.36(10)^{-12} \exp[-1710/T]$
42.	$2OH + M \rightarrow H_2O_2 + M$	$2.5(10)^{-33} \exp[2500/T]$
43.	$H_2O_2 + O(^3P) \rightarrow OH + HO_2$	$2.75(10)^{-12} \exp[-2125/T]$
44.	$CO + OH \rightarrow H + CO_2$	$\log_{10}K = -12.95 + 3.94(10)^{-4} T$
45.	$CH_2O + h\nu \rightarrow H_2 + CO$	J_{45}
46.	$CHO + O_2 \rightarrow HO_2 + CO$	$5(10)^{-12}$
47.	$CH_3 + O_2 + M \rightarrow CH_3O_2 + M$	$2.6(10)^{-31}$
48.	$CH_3O_2 + NO \rightarrow CH_3O + NO_2$	$1.5(10)^{-12} \exp[-500/T]$
49.	$CH_3O_2 + HO_2 \rightarrow CH_3O_2H + O_2$	$3.0(10)^{-11} \exp[-500/T]$
50.	$CH_3O_2H + h\nu \rightarrow CH_3O + OH$	J_{50}
51.	$CH_3O + O_2 \rightarrow CH_2O + HO_2$	$1.6(10)^{-13} \exp[-3300/T]$
52.	$CH_2O + h\nu \rightarrow H + CHO$	J_{52}
53.	$CH_2O + OH \rightarrow H_2O + CHO$	$1.4(10)^{-11}$

[a] Units in sec^{-1}, $cm^3 sec^{-1}$ and $cm^6 sec^{-1}$ for unimolecular, bimolecular and trimolecular reactions.

TABLE II. ADDITIONAL REACTIONS AND NEW NASA RATES

	REACTION	RATE COEFFICIENT[a]
7.	$O_3 + NO \rightarrow O_2 + NO_2$	$2.1\ 10^{-12} \exp[-1450/T]$
8.	$O_3 + NO_2 \rightarrow O_2 + NO_3$	$1.2\ 10^{-13} \exp[-2450/T]$
9.	$O_3 + OH \rightarrow O_2 + HO_2$	$1.5\ 10^{-12} \exp[-1000/T]$
10.	$NO + HO_2 \rightarrow OH + NO_2$	$8\ 10^{-12}$
12.	$OH + NO_2 + M \rightarrow HNO_3 + M$	$\log_{10}(k) = -AT/(B+T) - 0.5 \log_{10}(T/280)$
14.	$HO_2 + O_3 \rightarrow OH + O_2 + O_2$	$7.3\ 10^{-14} \exp[-1275/T]$
15.	$HO_2 + O \rightarrow OH + O_2$	$3.5\ 10^{-11}$
16.	$OH + HO_2 \rightarrow H_2O + O_2$	$3\ 10^{-11}$
17.	$OH + HNO_3 \rightarrow H_2O + NO_3$	$8\ 10^{-14}$
19.	$H_2O_2 + OH \rightarrow H_2O + HO_2$	$1\ 10^{-11} \exp[-750/T]$
20.	$HO_2 + HO_2 \rightarrow H_2O_2 + O_2$	$2.5\ (10)^{-12}$
24.	$N_2O + O(^1D) \rightarrow N_2 + O_2$	$5.5\ 10^{-11}$
25.	$N_2O + O(^1D) \rightarrow NO + NO$	$5.5\ 10^{-11}$
27.	$N + O_2 \rightarrow NO + O$	$5.5\ (10)^{-12} \exp[-3220/T]$
28.	$N + NO \rightarrow N_2 + O$	$8.2\ 10^{-11} \exp[-410/T]$
30.	$N_2 + O(^1D) + M \rightarrow N_2O + M$	$3.5\ 10^{-37}$
31.	$NO_2 + N \rightarrow N_2O + O$	$2\ 10^{-11} \exp[-800/T]$
34.	$OH + O \rightarrow O_2 + H$	$4.2\ 10^{-11}$
37.	$NO + O + M \rightarrow NO_2 + M$	$1.55\ 10^{-32} \exp[584/T]$
39.	$N + O_3 \rightarrow NO + O_2$	$5\ 10^{-12} \exp[-650/T]$
42.	$2OH + M \rightarrow H_2O_2 + M$	$1.25\ 10^{-32} \exp[900/T]$
44.	$CO + OH \rightarrow H + CO_2$	$1.4\ 10^{-13}$
46.	$CHO + O_2 \rightarrow HO_2 + CO$	$6\ 10^{-12}$
48.	$CH_3O_2 + NO \rightarrow CH_3O + NO_2$	$1.5\ 10^{-12}$
49.	$CH_3O_2 + HO_2 \rightarrow CH_3O_2H + O_2$	$2.5\ 10^{-12}$

	REACTION	RATE COEFFICIENT[a]
53.	$CH_2O + OH \rightarrow H_2O + CHO$	$3\ 10^{-11} \exp[-250/T]$
54.	$NO_3 + NO_2 + M \rightarrow N_2O_5 + M$	$1.9\ 10^{-30}(3+5C) / \lvert(1+5C)(3+C)\rvert$ $C = 5\ 10^{-19}[M]$
55.	$N_2O_5 + M \rightarrow NO_3 + NO_2 + M$	$D(4+6F) / \lvert(1+6F)(4+F)\rvert$ $D = 2.2\ 10^{-5} \exp[-9700/T]$ $E = 5.7\ 10^{14} \exp[-10600/T]$ $F = B[M]/E$
56.	$NO_3 + h\nu \rightarrow 2/3(NO_2 + O) + 1/3(NO + O_2)$	
57.	$N_2O_5 + h\nu \rightarrow NO_2 + NO_3$	
58.	$NO_3 + NO \rightarrow 2NO_2$	$8.7\ 10^{-12}$
59.	$NO_2 + O + M \rightarrow NO_3 + M$	$1\ 10^{-31}$
60.	$CO_2 + h\nu \rightarrow O + CO$	
61.	$H_2 + O(^1D) \rightarrow OH + H$	$9.9\ 10^{-11}$
62.	$O(^1D) + CH_4 \rightarrow H_2 + CH_2O$	$1.4\ 10^{-11}$
63.	$O + CH_4 \rightarrow CH_3 + OH$	$3.5\ 10^{-11} \exp[-4450/T]$
64.	$CH_2O + O \rightarrow OH + CHO$	$2\ 10^{-11} \exp[-1450/T]$
	$A = A_1 + A_2 z + A_3 z^2 + A_4 z^3$	
	$B = B_1 + B_2 z + B_3 z^2$	
	$A_1 = 31.62273$	$B_1 = -327.372$
	$A_2 = -0.258304$	$B_2 = 44.5586$ $z = \log_{10}\lvert 0.94[N_2]\rvert$
	$A_3 = -0.0889287$	$B_3 = -1.38092$
	$A_4 = 2.520173(10)^{-3}$	

[a] Units in sec^{-1}, $cm^3 sec^{-1}$ and $cm^6 sec^{-1}$ for unimolecular, bimolecular and trimolecular reactions.

*TABLE III. - 1990 WORLDWIDE AIRCRAFT NO_x EMISSIONS, HIGH ESTIMATES, kg/yr

Latitude	6-8	8-9	9-10	10-11	11-12	12-13	13-14	14-15	15-16	16-17	17-18	18-19	Total
N 60+	3.35E6	3.03E6	1.43E7	1.31E7	1.46E7	1.31E6	9.99E5	4.06E5	1.72E6	2.59E6	2.10E6	1.43E6	5.894E7
50-60	2.15E7	2.59E7	9.44E7	1.06E8	9.09E7	8.26E6	3.72E6	2.12E6	6.57E6	1.03E7	8.06E6	3.71E6	3.814E8
40-50	7.60E7	8.70E7	1.79E8	2.79E8	1.62E8	2.48E7	4.59E6	2.09E6	4.17E6	6.96E6	5.46E6	2.36E6	8.334E8
30-40	7.74E7	9.20E7	1.67E8	3.09E8	1.72E8	2.97E7	3.11E6	1.74E6	1.30E6	2.73E6	2.07E6	8.63E5	8.589E8
20-30	2.61E7	2.83E7	6.74E7	1.02E8	6.92E7	8.73E6	1.55E6	1.20E6	8.06E5	1.90E6	1.71E6	4.67E5	3.094E8
10-20	1.11E7	1.18E7	2.65E7	4.28E7	3.99E7	3.67E6	4.74E5	1.54E5	3.24E5	5.38E5	4.22E5	1.71E5	1.379E8
0-10	4.80E6	5.14E6	1.50E7	1.82E7	1.36E7	1.26E6	1.73E5	0	2.91E5	4.08E5	3.44E5	1.63E5	5.938E7
10-0	3.31E6	3.77E6	1.22E7	1.38E7	1.09E7	8.65E5	1.38E5	0	3.01E5	4.22E5	3.56E5	1.65E5	4.623E7
20-10	2.74E6	3.21E6	1.14E7	1.52E7	1.15E7	1.11E6	3.15E5	1.32E5	1.10E5	2.19E5	1.58E5	7.52E4	4.617E7
30-20	3.67E6	4.01E6	9.47E6	1.37E7	8.66E6	9.31E5	5.10E4	0	9.85E4	1.38E5	1.16E5	6.63E4	4.091E7
40-30	4.01E6	4.63E6	6.62E6	1.18E7	6.14E6	1.21E6	8.64E4	5.16E4	1.56E4	4.74E4	2.84E4	6.22E3	3.464E7
50-40	2.36E5	3.05E5	3.19E5	8.28E5	4.46E5	9.29E4	1.5 E1	0	0	0	0	0	2.227E6
60-50	4.77E4	3.79E4	2.99E4	2.52E4	1.04E4	1.45E3	0.97	0	0	0	0	0	1.526E5
S 60+	0	0	0	0	0	0	0	0	0	0	0	0	0
Total	2.343E8	2.691E8	6.036E8	9.255E8	5.999E8	8.197E7	1.521E7	7.894E6	1.571E7	2.625E7	2.082E7	9.477E6	2.810E9

*Oliver, R.C., et al. (ref. 35)

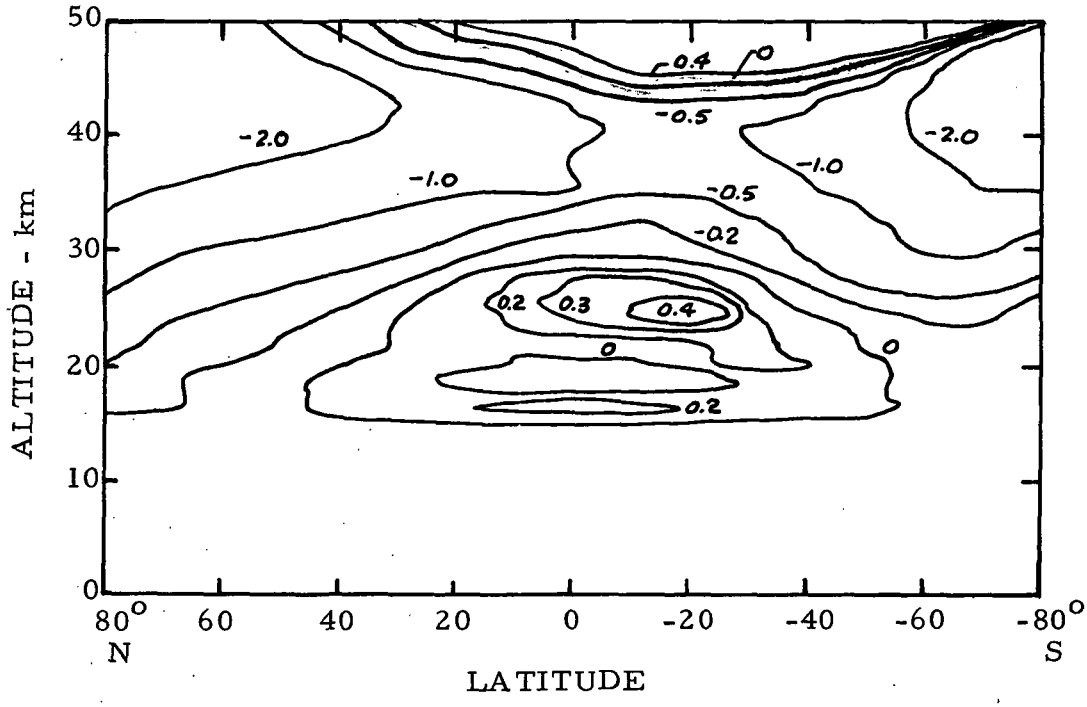

(a) PRESENT MODEL

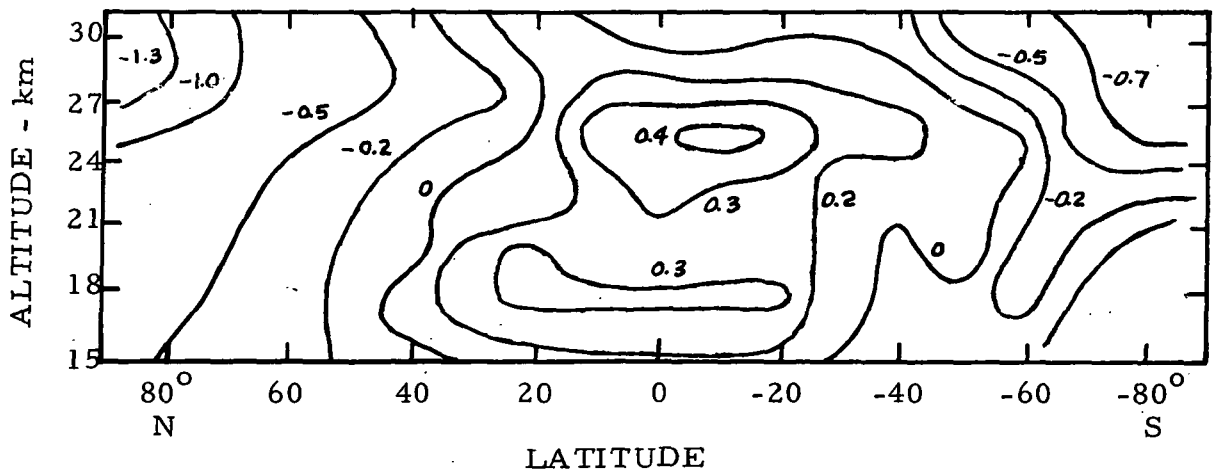

(b) DOPPLICK (REF. 6)

FIG. 1. FALL SEASON NET RADIATIVE HEATING (^{o}K/DAY)

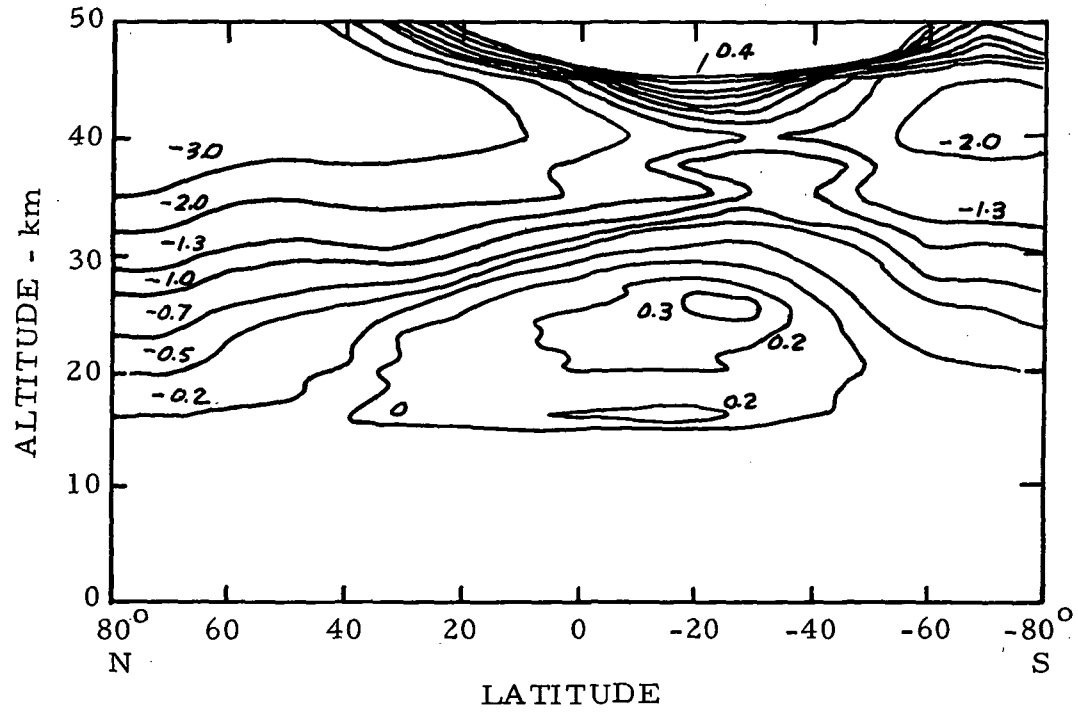

FIG. 2. WINTER SEASON NET RADIATIVE HEATING ($^{\circ}$K/DAY)

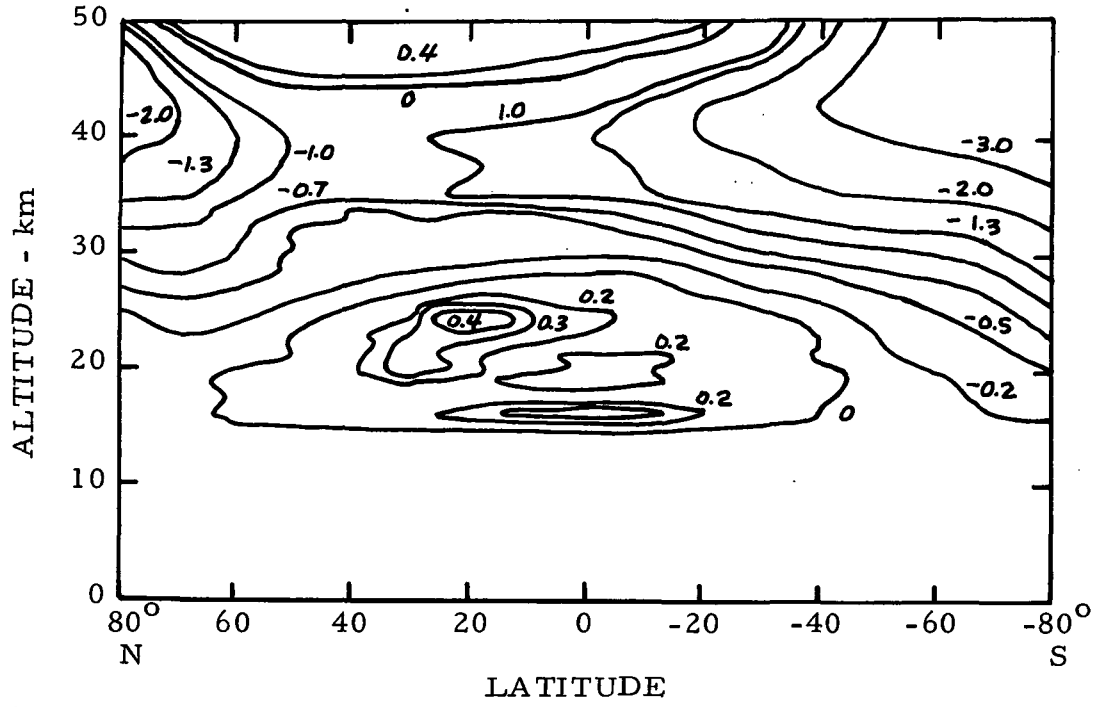

FIG. 3. SPRING SEASON NET RADIATIVE HEATING (°K/DAY)

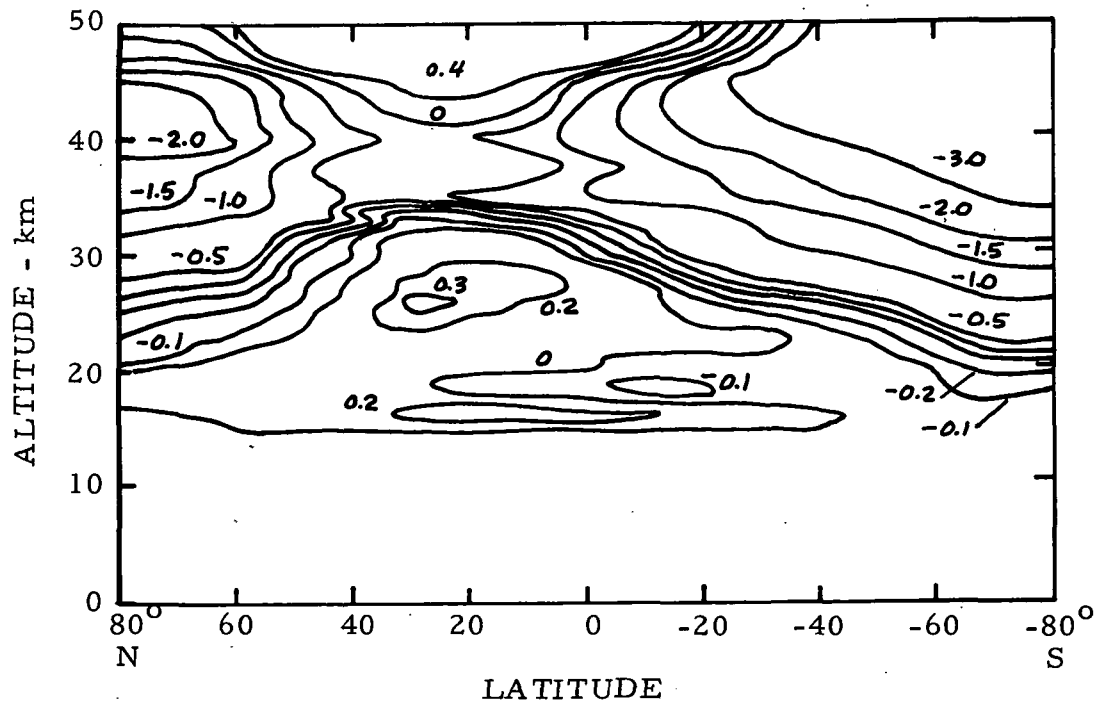

FIG. 4. SUMMER SEASON NET RADIATIVE HEATING (°K/DAY)

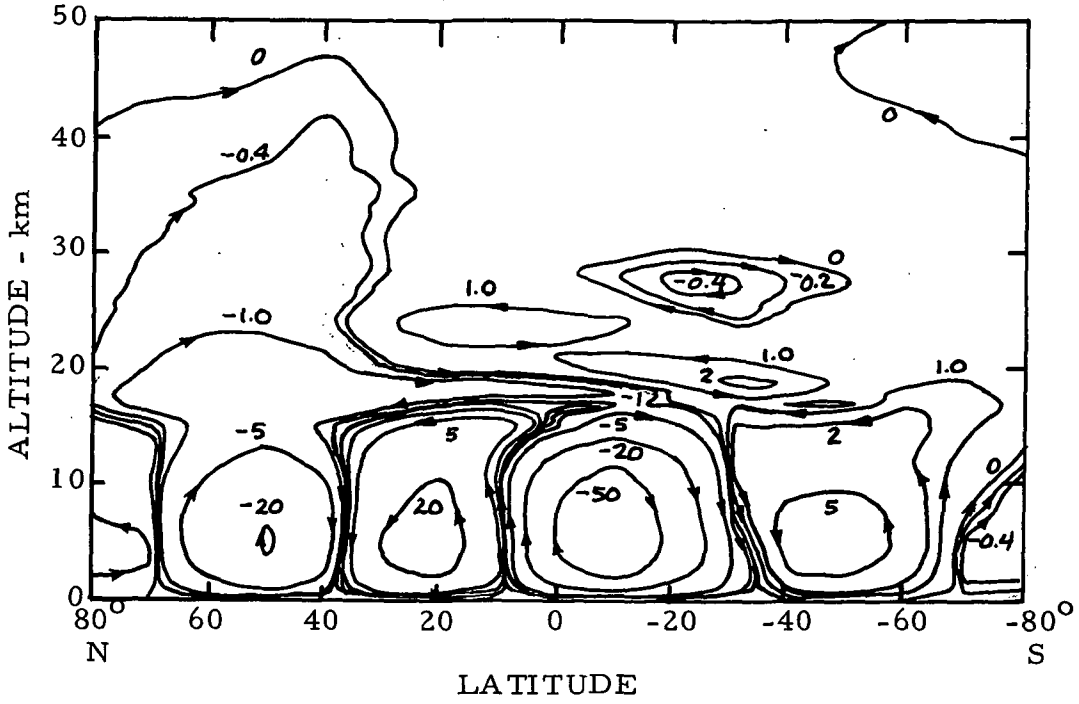

(a) PRESENT MODEL

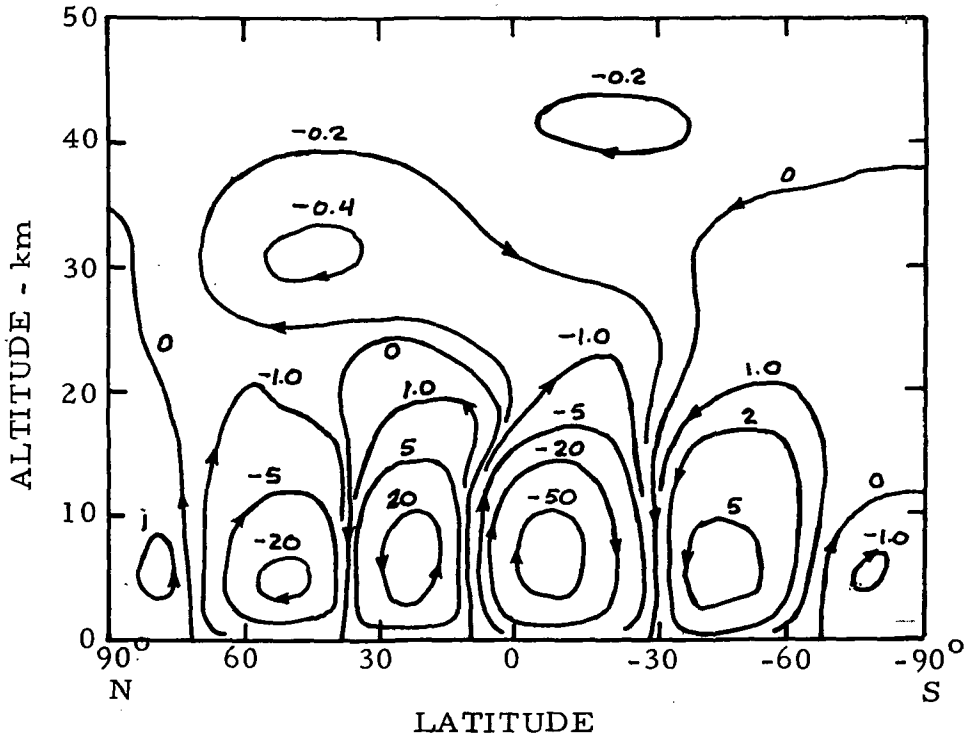

(b) LOUIS (REF. 5)

FIG. 5. FALL SEASON INTEGRATED MASS FLUX (10^{12} gm/sec)

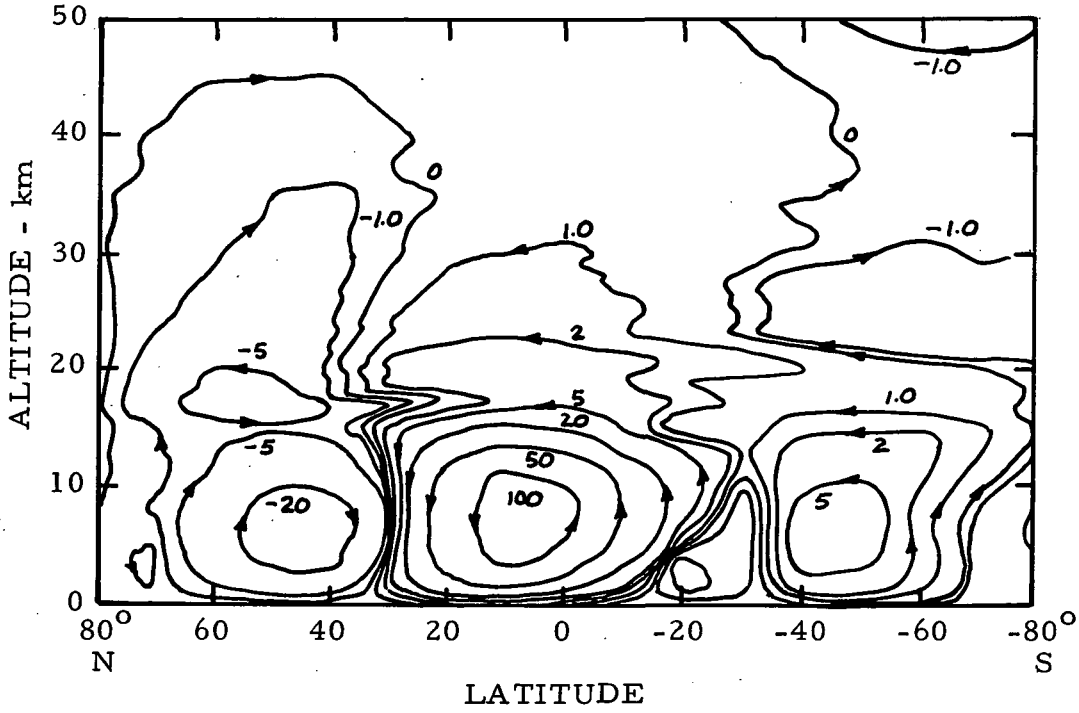

(a) PRESENT MODEL

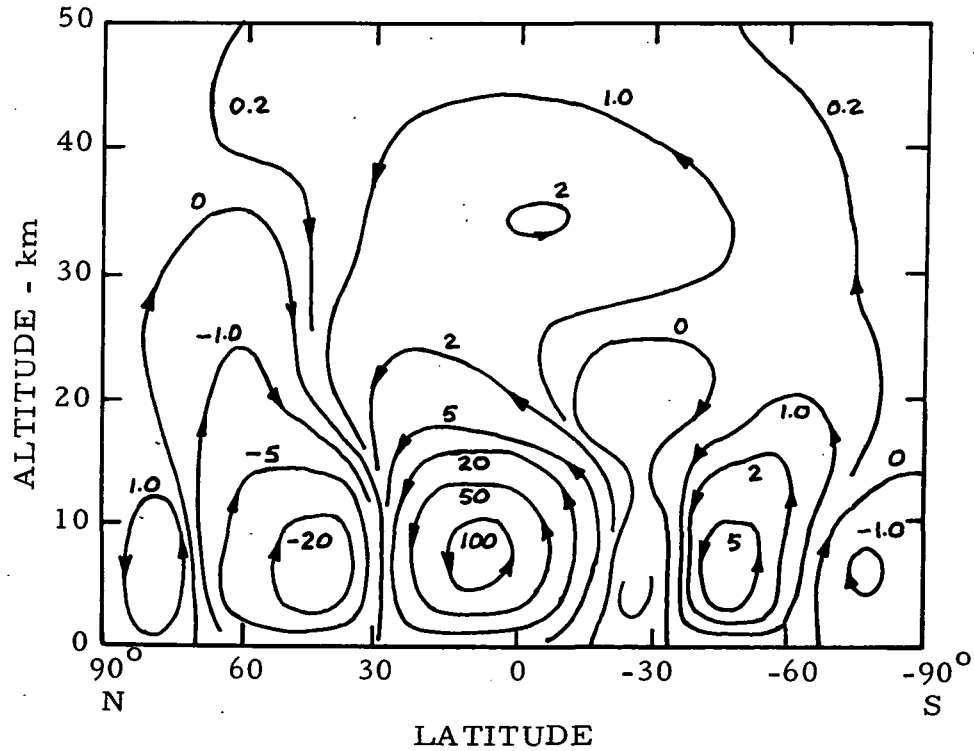

(b) LOUIS (REF. 5)

FIG. 6. WINTER SEASON INTEGRATED MASS FLUX (10^{12} gm/sec)

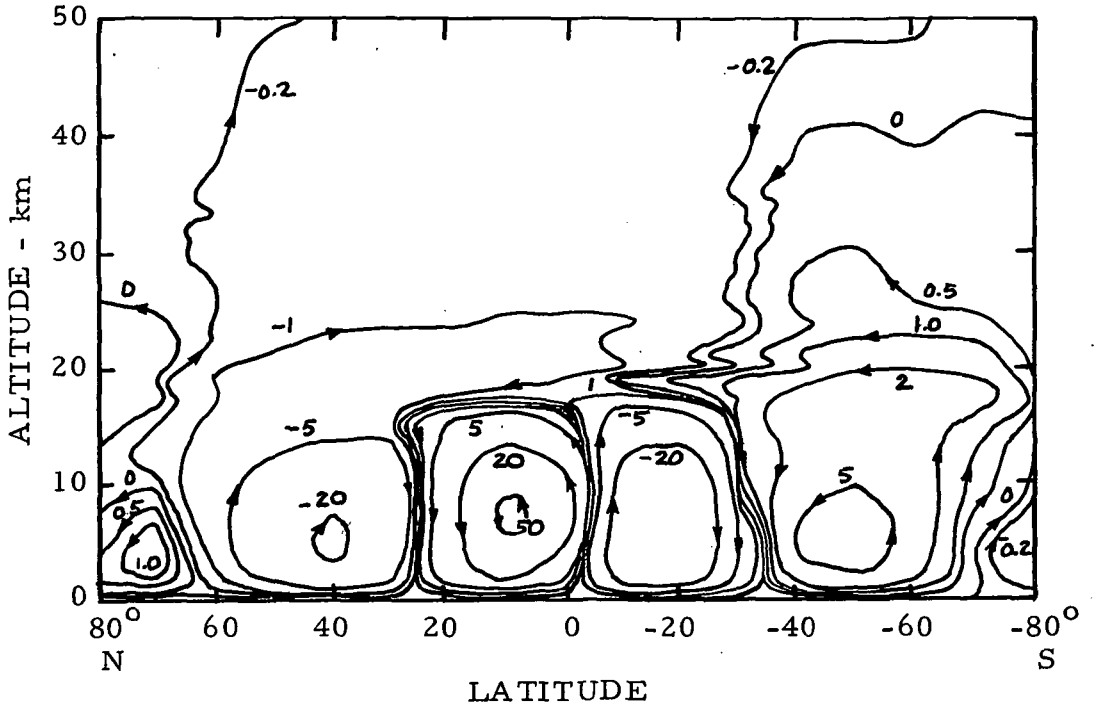

(a) PRESENT MODEL

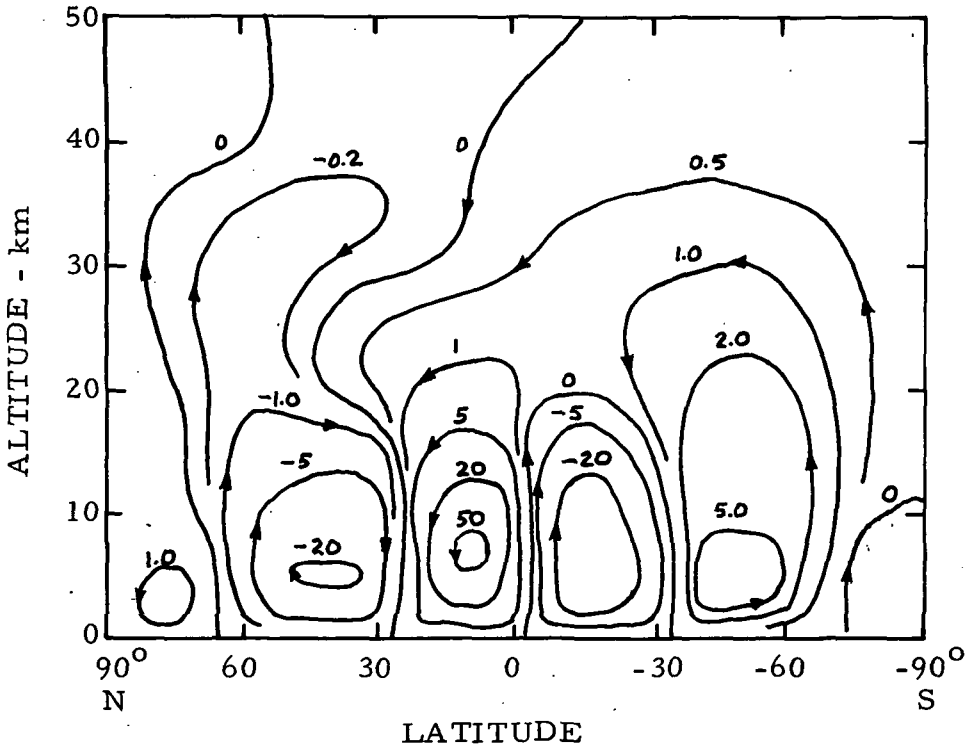

(b) LOUIS (REF. 5)

FIG. 7. SPRING SEASON INTEGRATED MASS FLUX (10^{12} gm/sec)

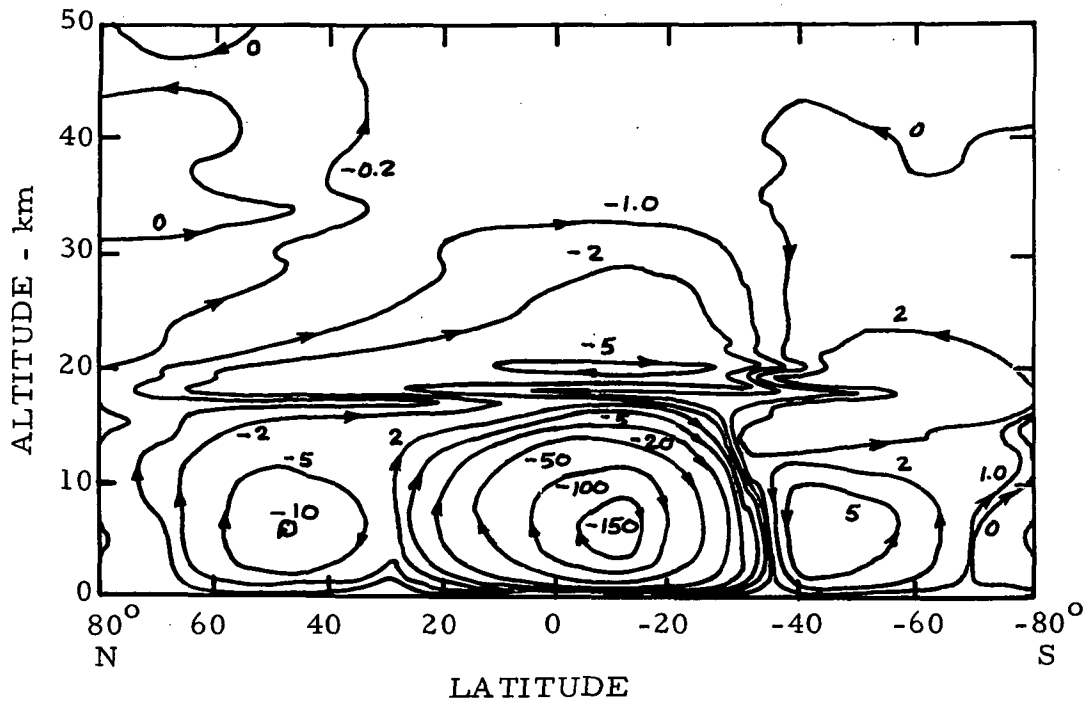

(a) PRESENT MODEL

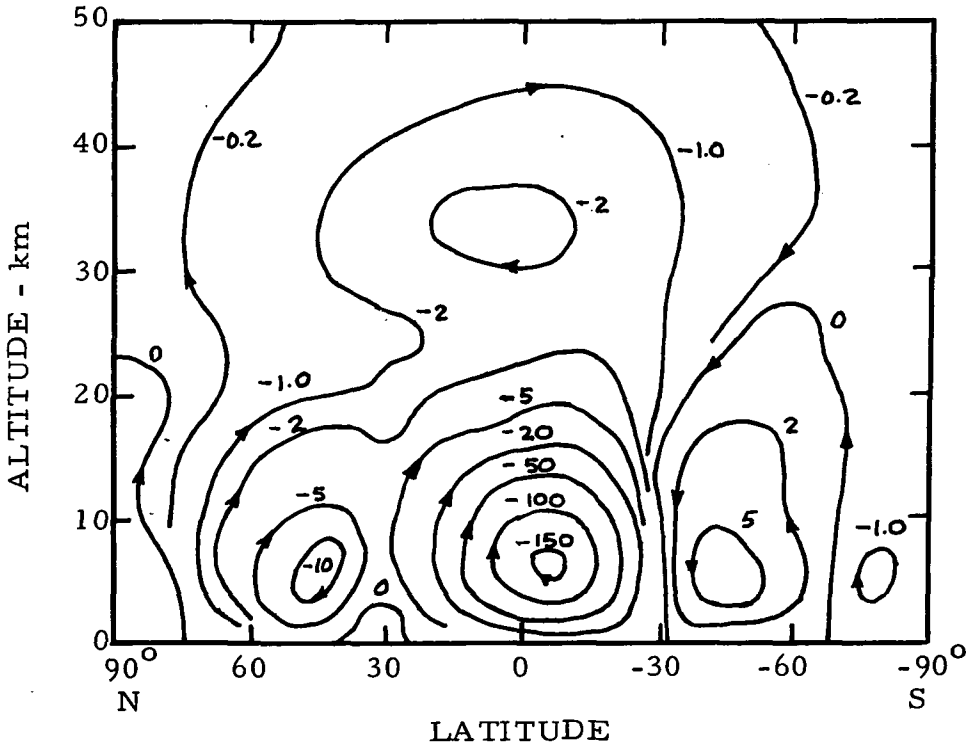

(b) LOUIS (REF. 5)

FIG. 8. SUMMER SEASON INTEGRATED MASS FLUX (10^{12} gm/sec)

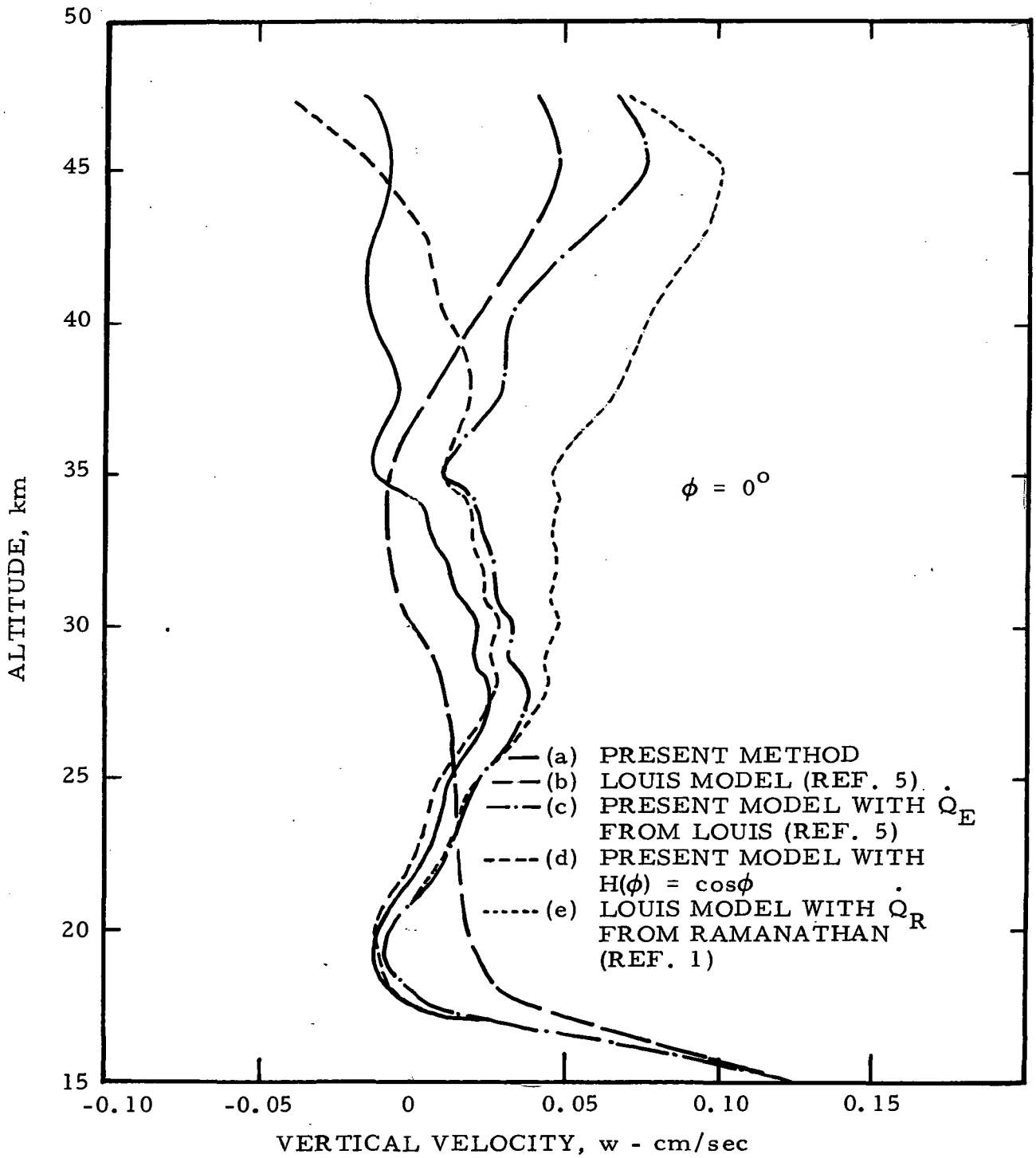

FIG. 9. FALL SEASON VERTICAL VELOCITY PROFILE AT $\phi = 0^{o}$N

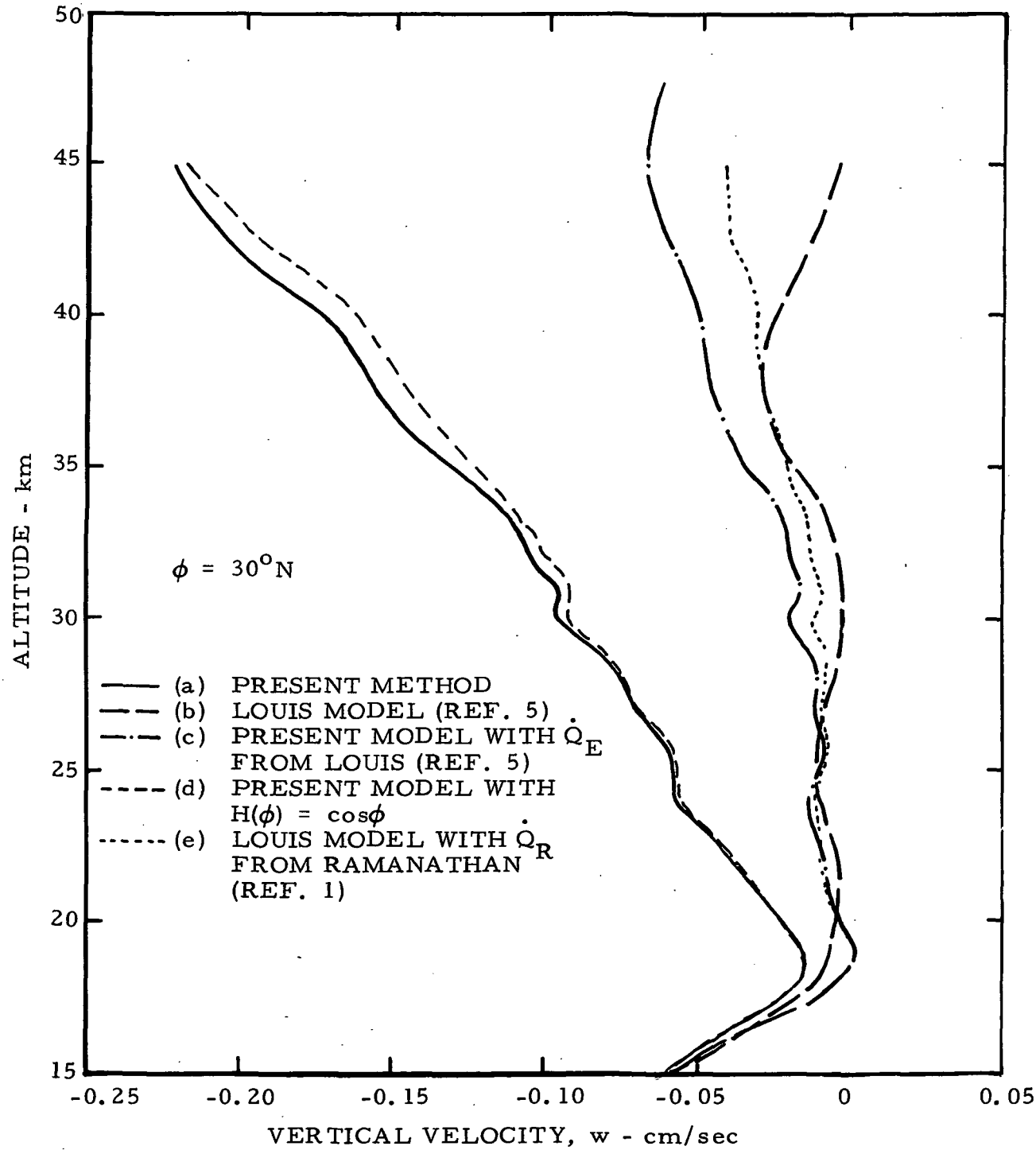

FIG. 10. FALL SEASON VERTICAL VELOCITY PROFILE AT ϕ = 30°N

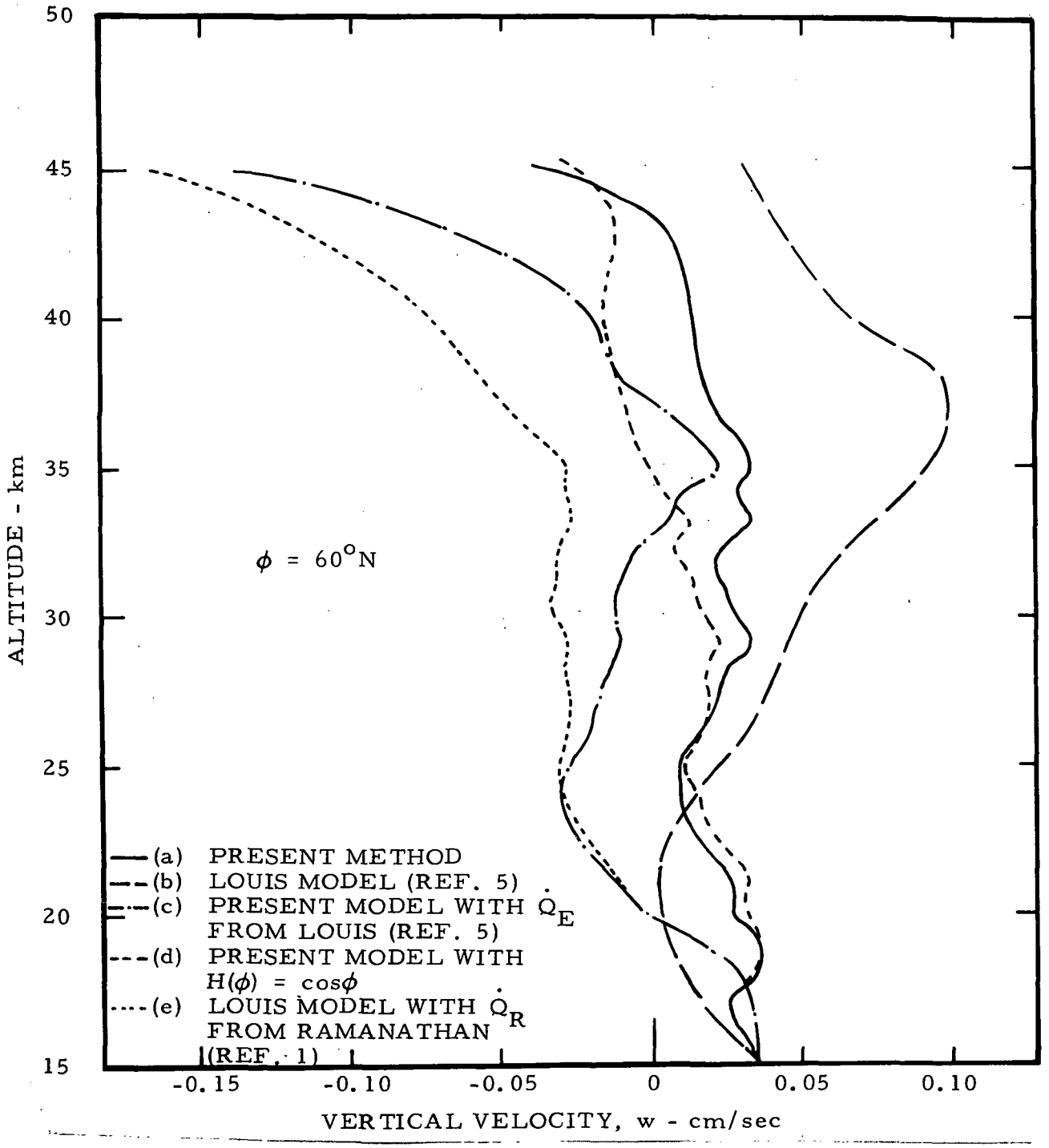

FIG. 11. FALL SEASON VERTICAL VELOCITY PROFILE AT ϕ = 60°N

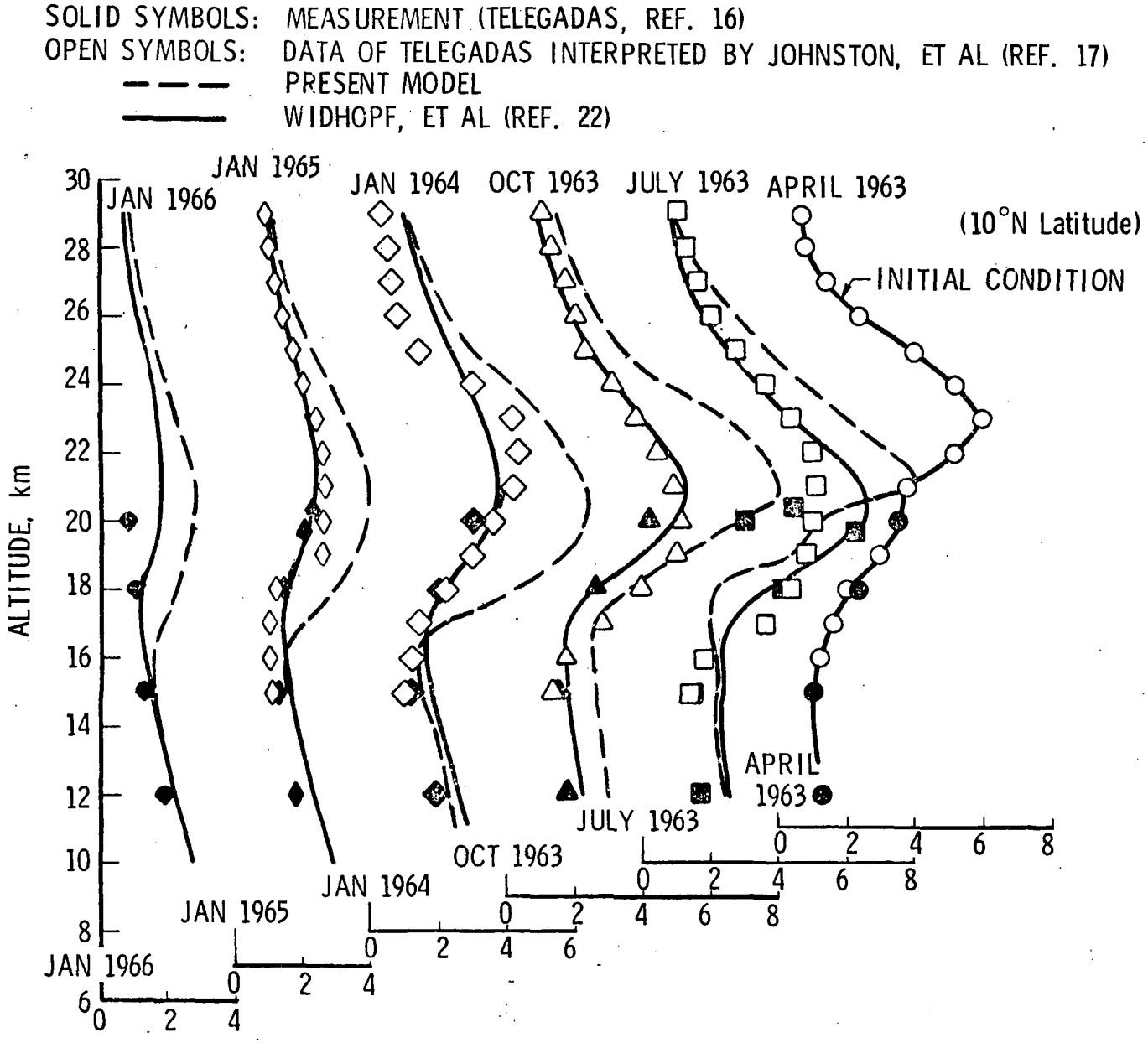

FIG. 12. CONCENTRATION OF EXCESS CARBON-14 AT $\phi = 10^{\circ}N$ (10^3 molecules/cm^3)

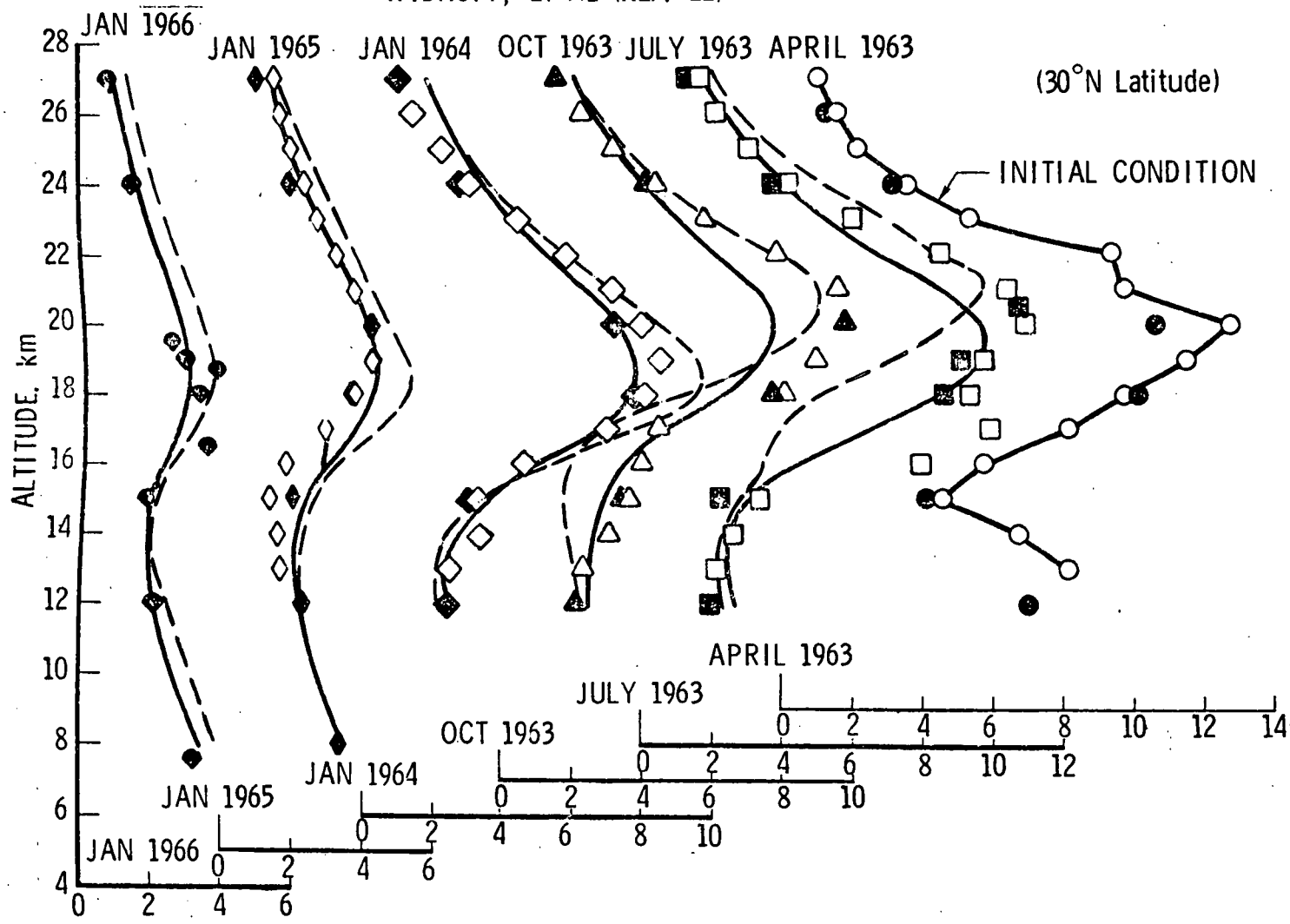

FIG. 13. CONCENTRATION OF EXCESS CARBON-14 AT $\phi = 30^{\circ}N$ (10^3 molecules/cm^3)

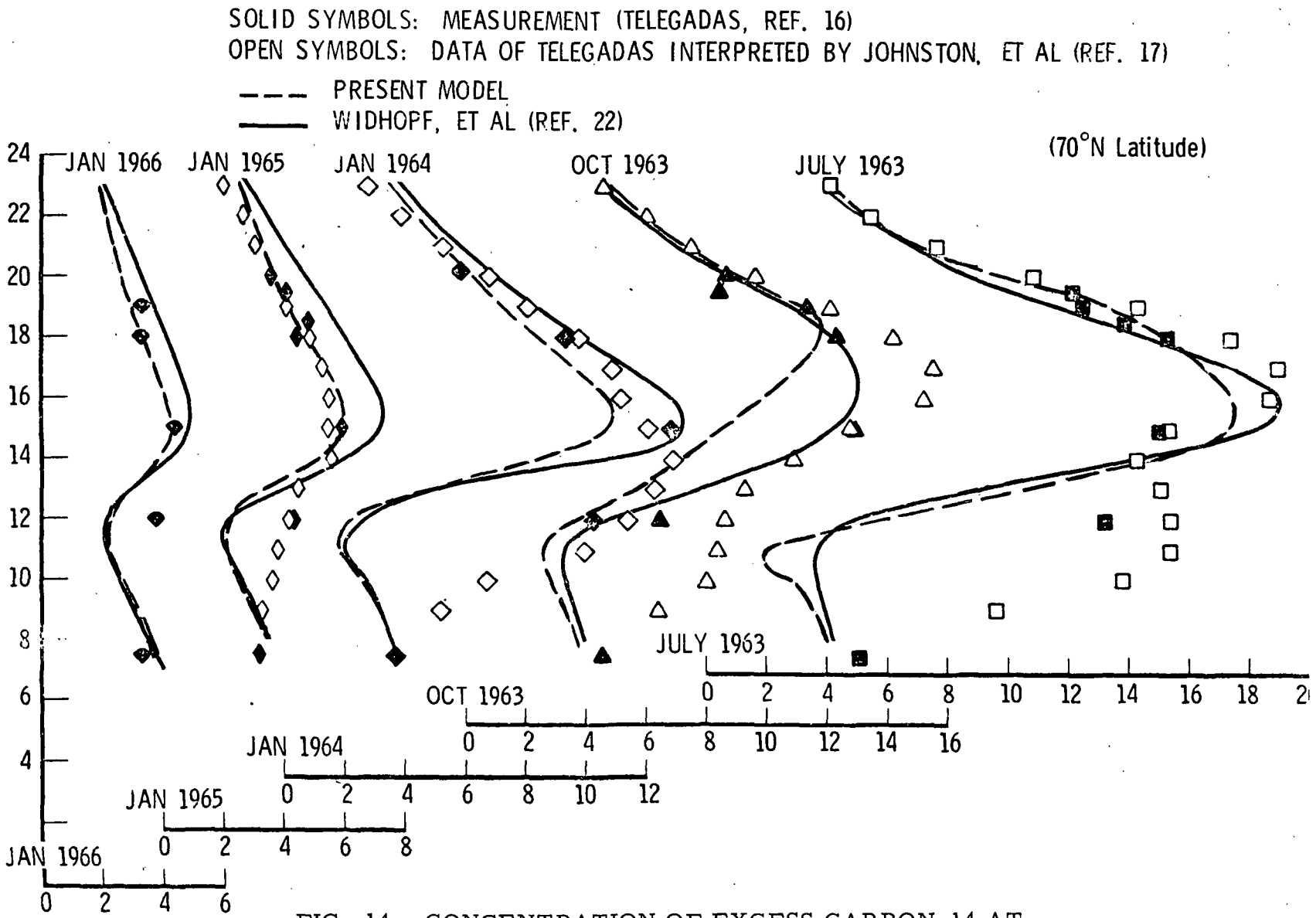

FIG. 14. CONCENTRATION OF EXCESS CARBON-14 AT $\phi = 70^{o}N$ (10^3 molecules/cm^3)

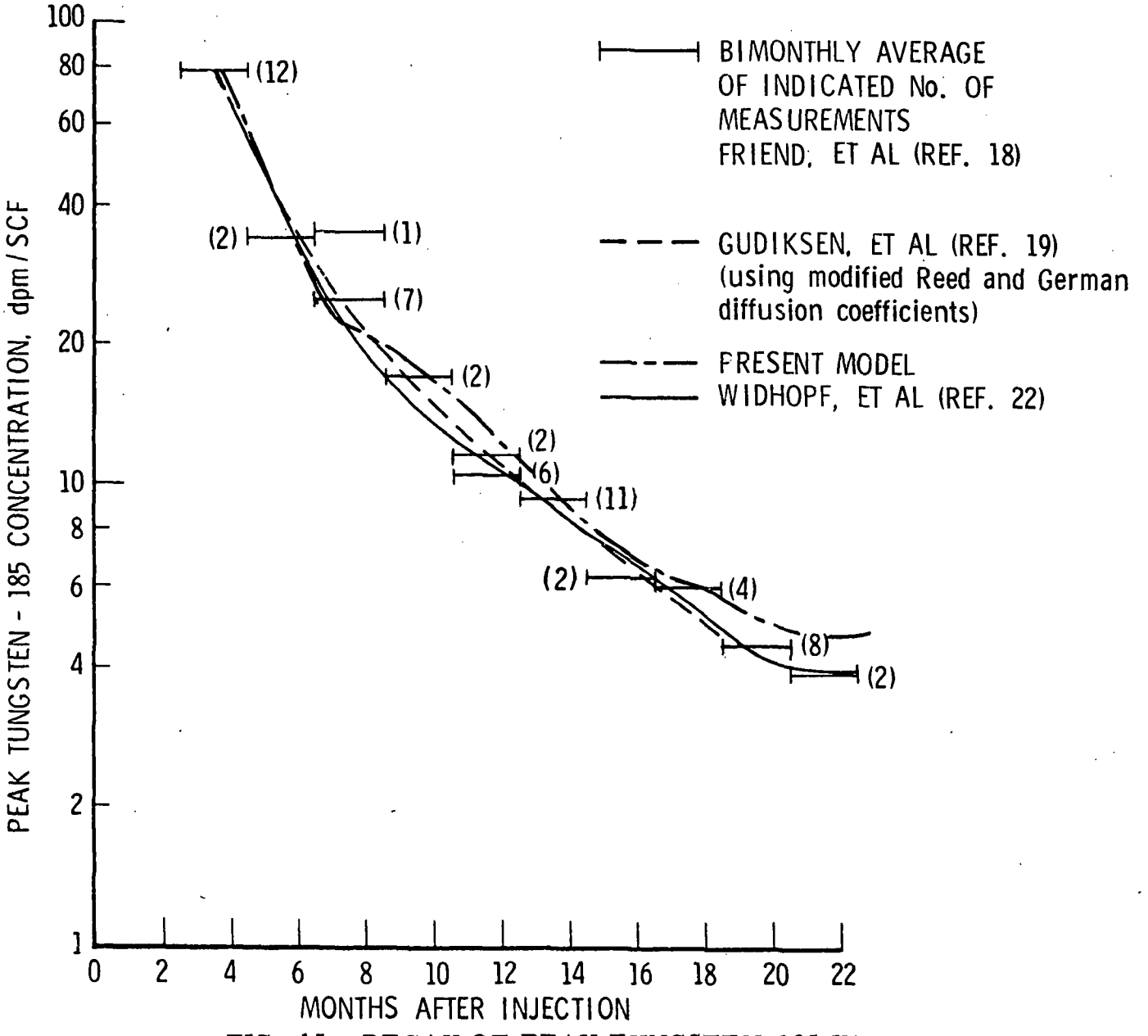

FIG. 15. DECAY OF PEAK TUNGSTEN-185 IN EQUATORIAL REGION (dpm/SCF)

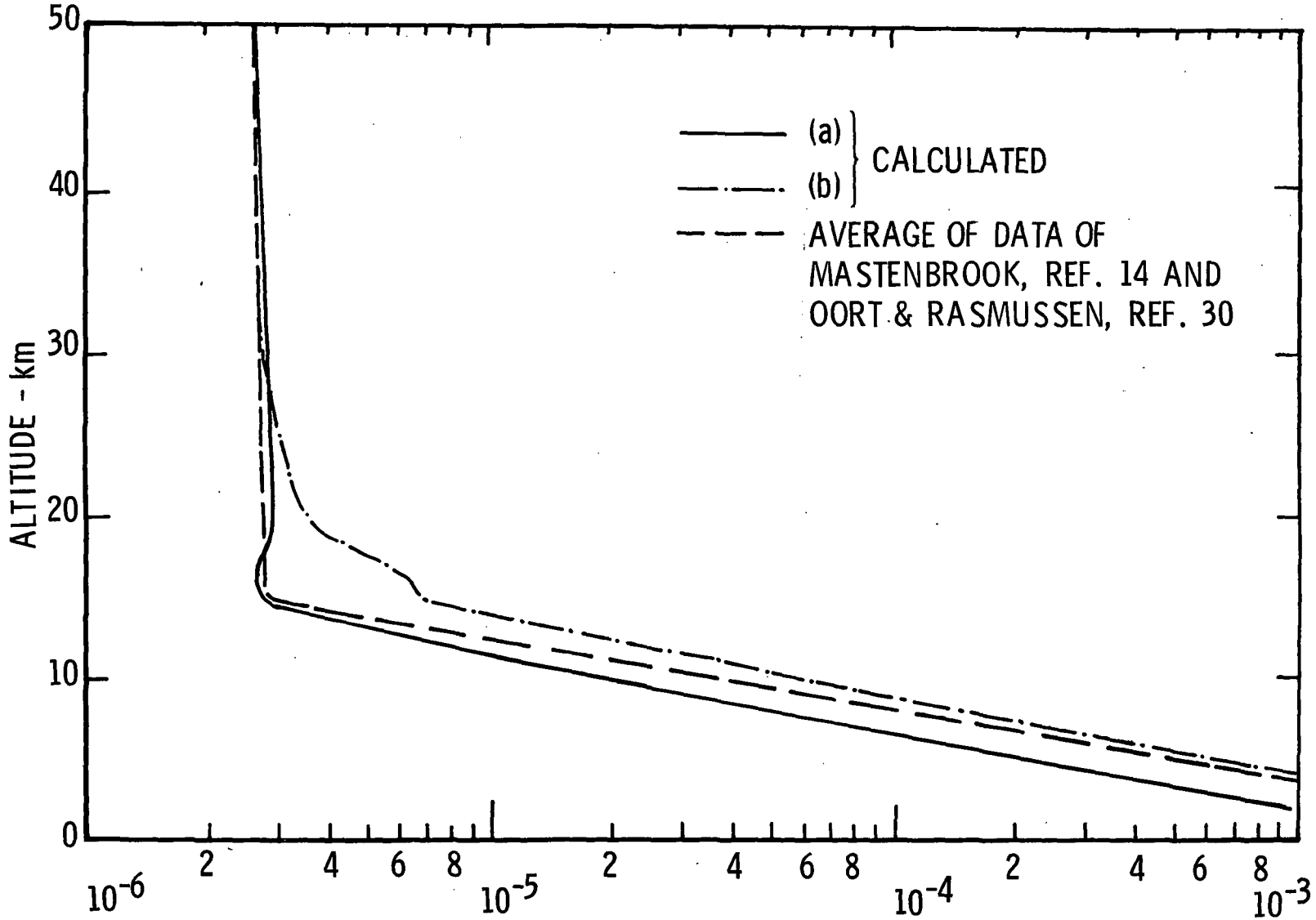

FIG. 16. 1-D WATER VAPOR PROFILE

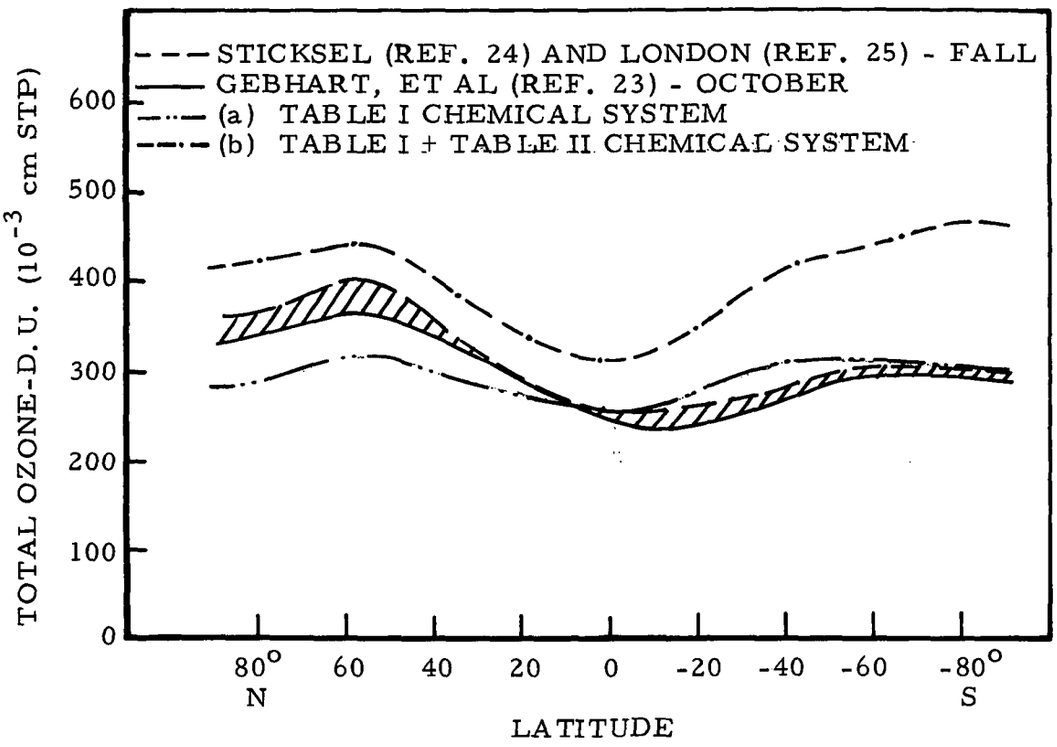

FIG. 17. TOTAL OZONE COLUMN DISTRIBUTION FOR THE NATURAL ATMOSPHERE DURING THE FALL SEASON

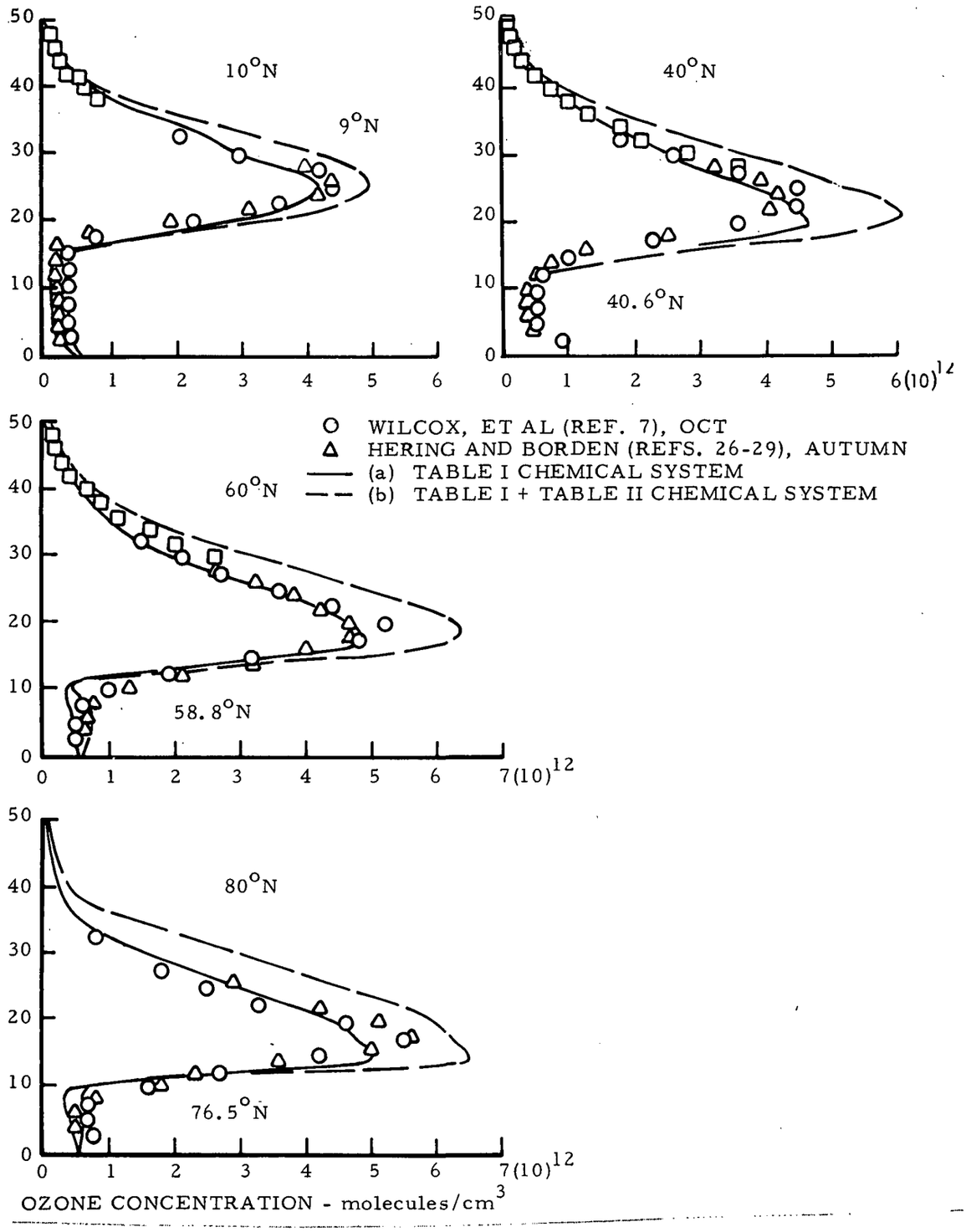

FIG. 18. FALL SEASON OZONE PROFILES IN THE NATURAL ATMOSPHERE

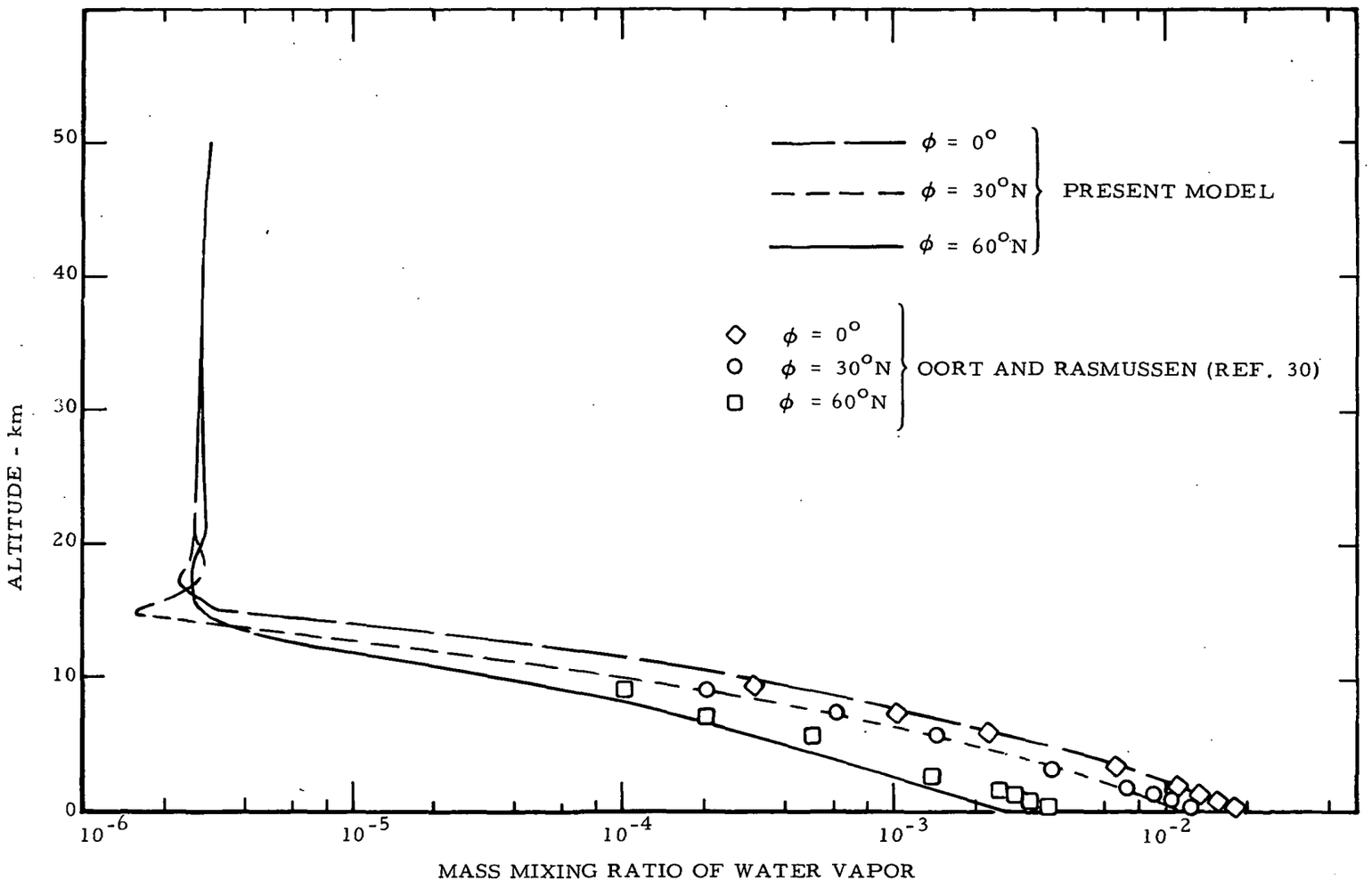

FIG. 19. FALL SEASON WATER VAPOR PROFILES IN THE NATURAL ATMOSPHERE

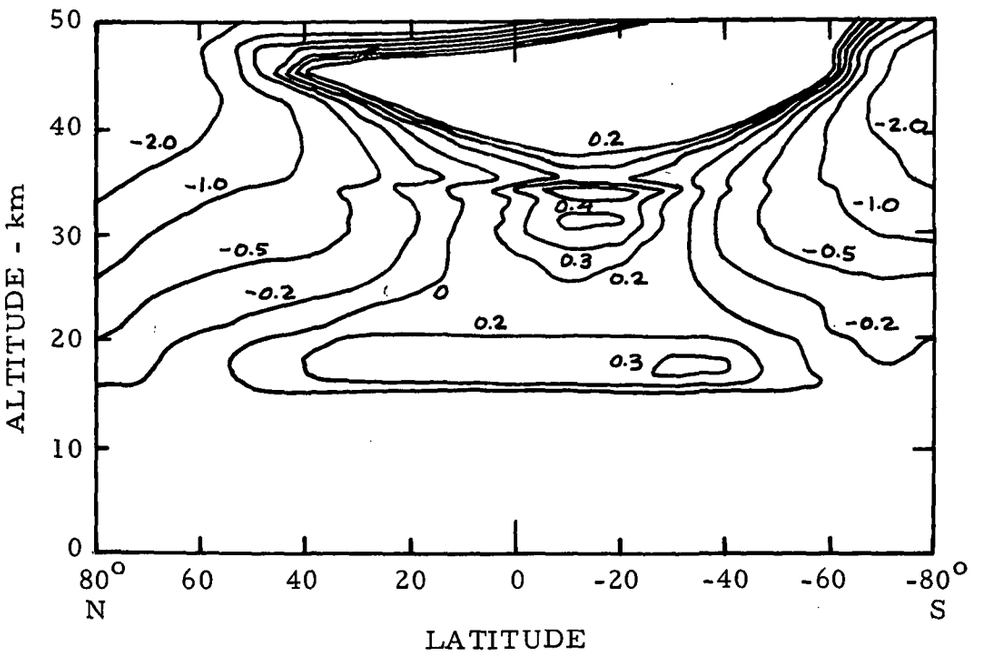

FIG. 20. FALL SEASON NET RADIATIVE HEATING (°K/DAY) FOR THE NATURAL ATMOSPHERE

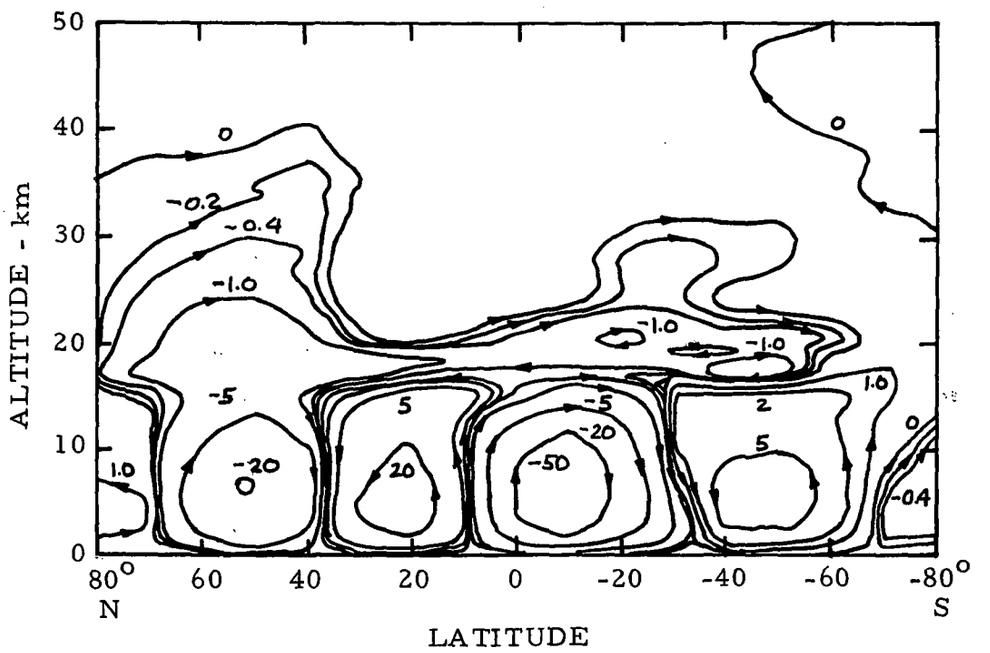

FIG. 21. FALL SEASON INTEGRATED MASS FLUX (10^{12} gm/sec) FOR THE NATURAL ATMOSPHERE

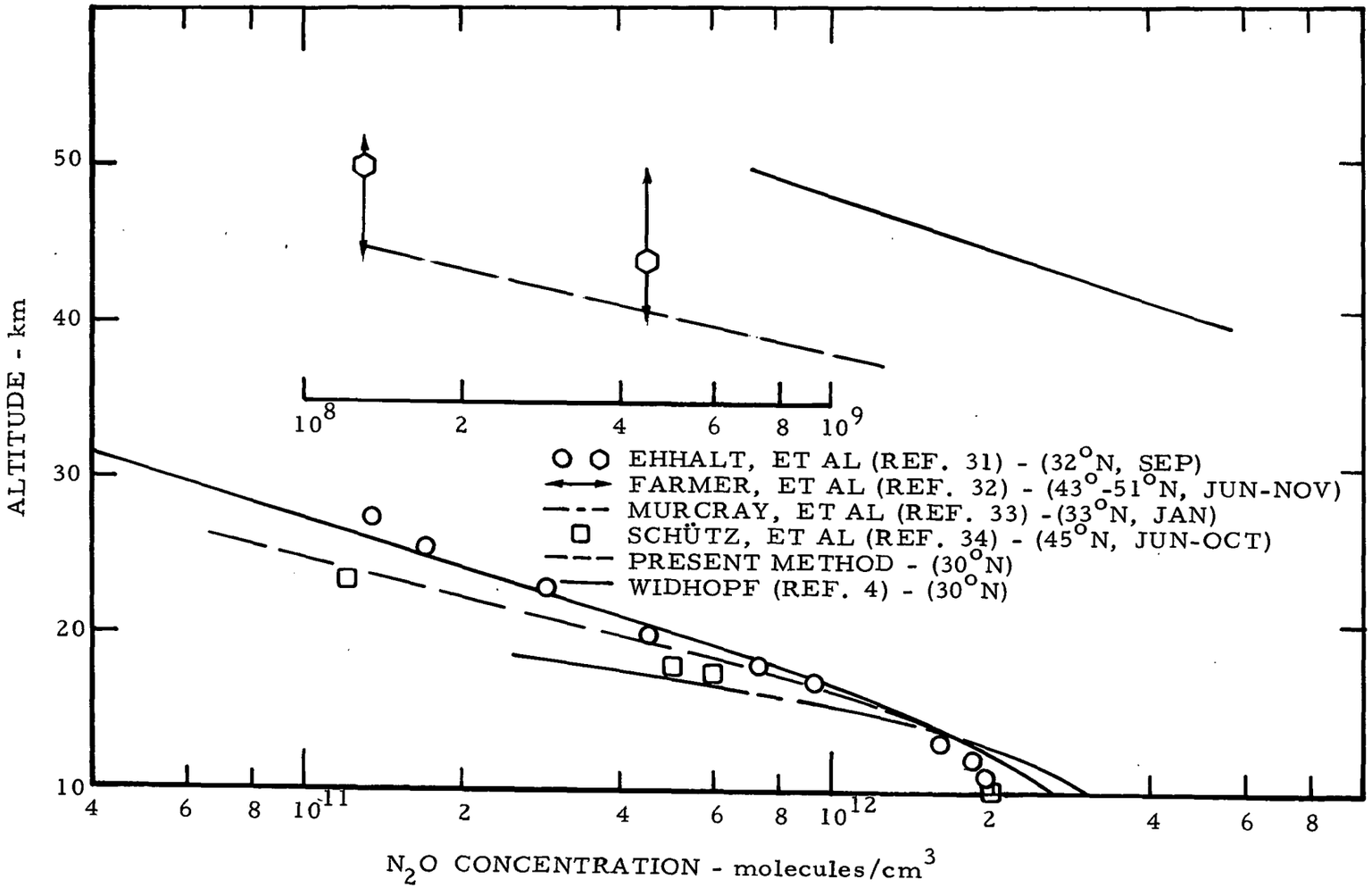

FIG. 22. N_2O PROFILES FOR NATURAL ATMOSPHERE DURING FALL SEASON (molecules/cm^3)

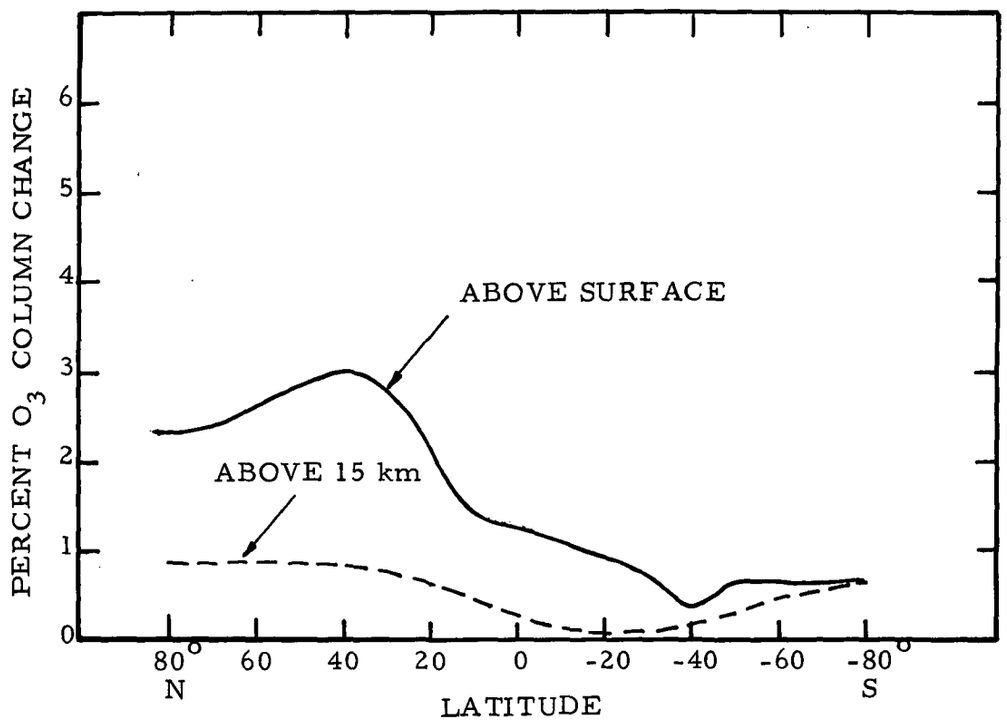

FIG. 23. PERCENT OZONE CHANGE DISTRIBUTION FOR $NO_x + HO_x$ INJECTION CASE DURING THE FALL SEASON

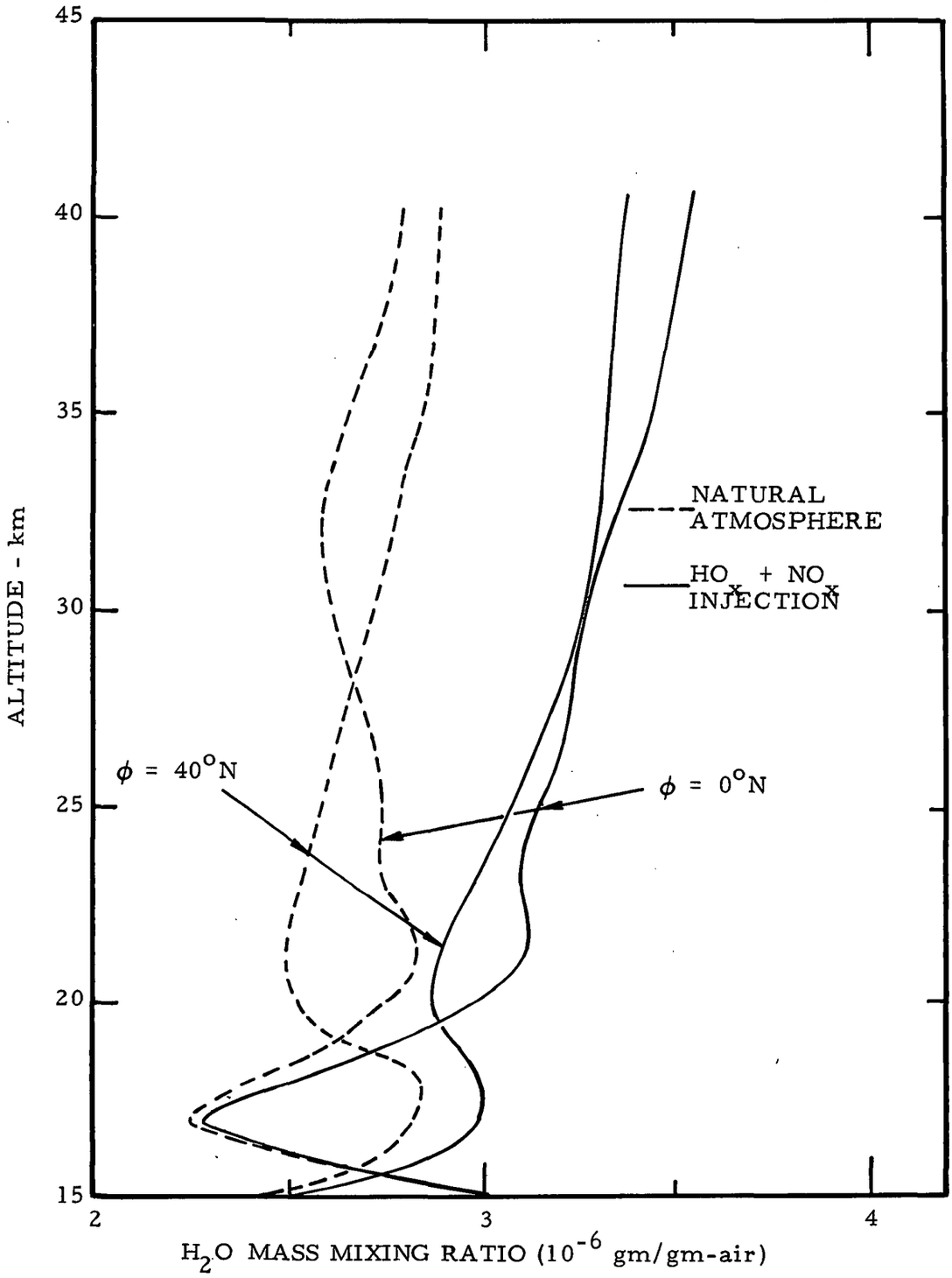

FIG. 24. WATER VAPOR PROFILES FOR HO_x + NO_x INJECTION DURING THE FALL SEASON

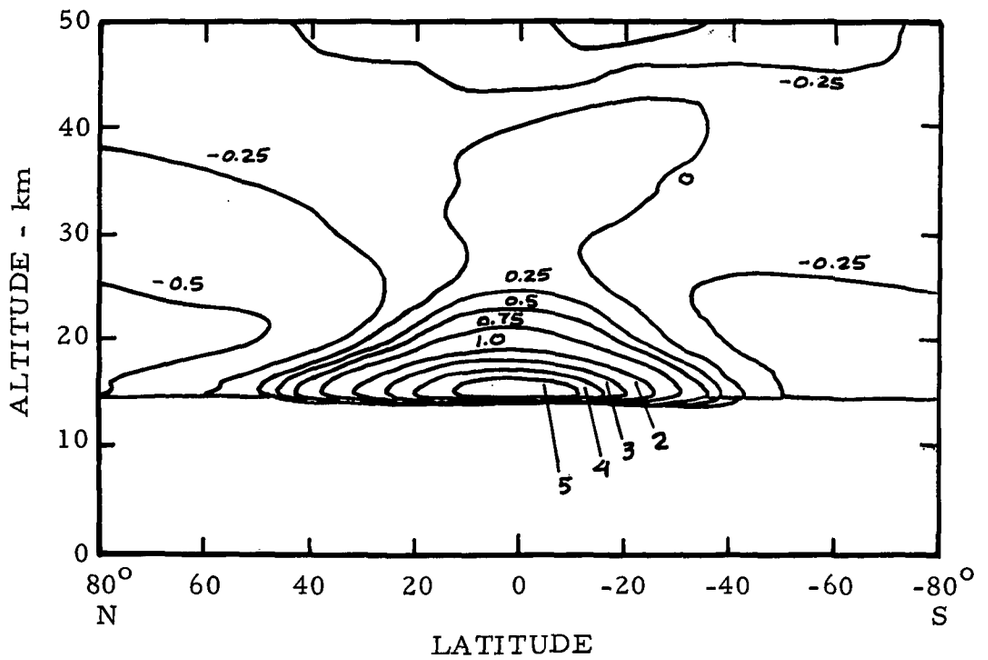

FIG. 25. TEMPERATURE PERTURBATION FOR NO_x + HO_x INJECTION CASE (°K) DURING THE FALL SEASON

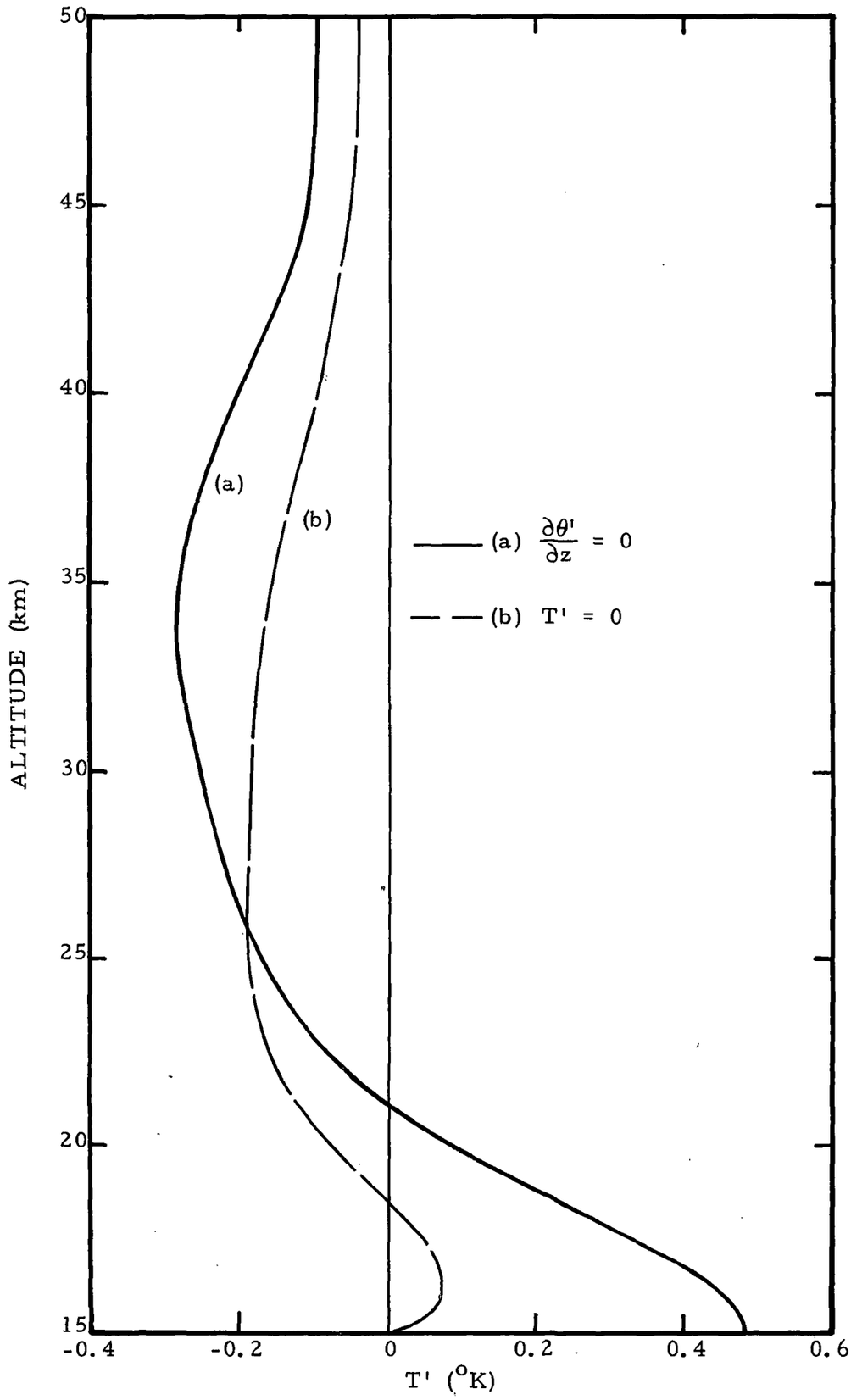

FIG. 26. VERTICAL DISTRIBUTION OF THE TEMPERATURE PERTURBATION (30°N) CALCULATED USING A ONE-DIMENSIONAL MODEL

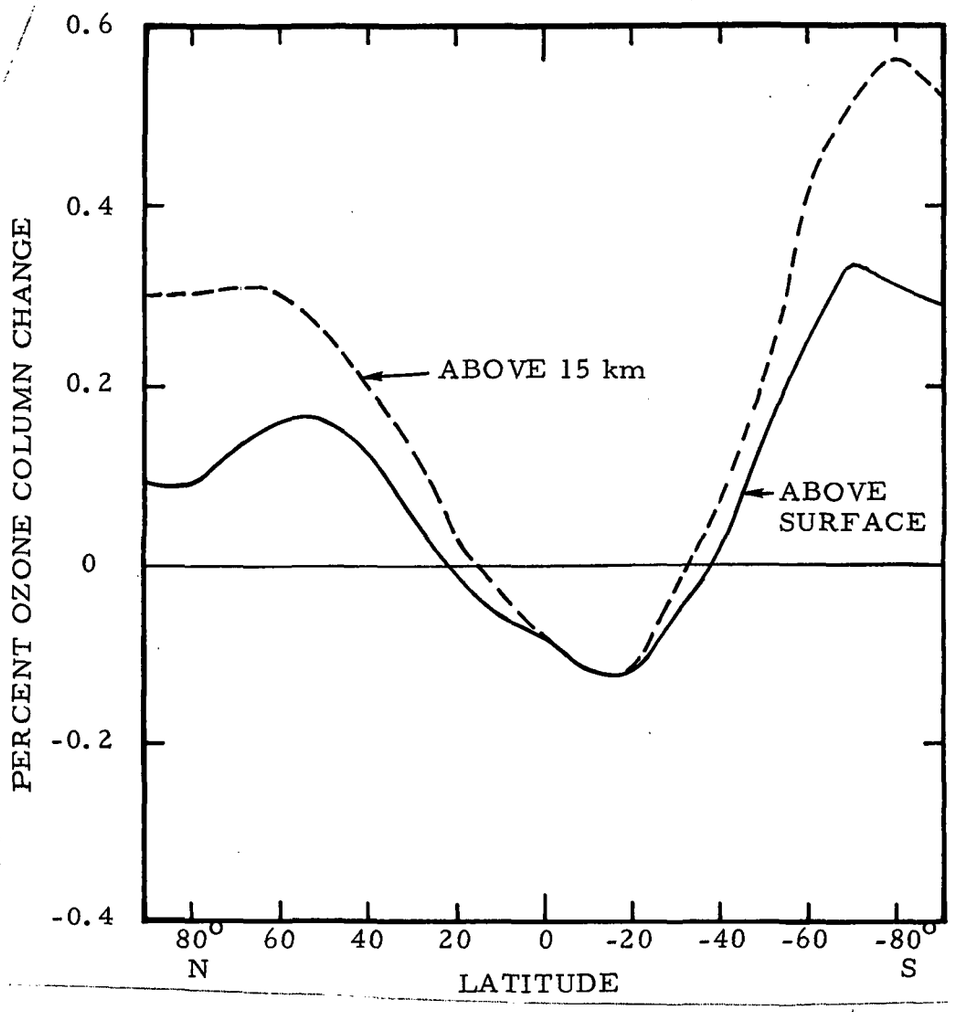

FIG. 27. OZONE COLUMN CHANGE FOR H_2O INJECTION CASE DURING THE FALL SEASON

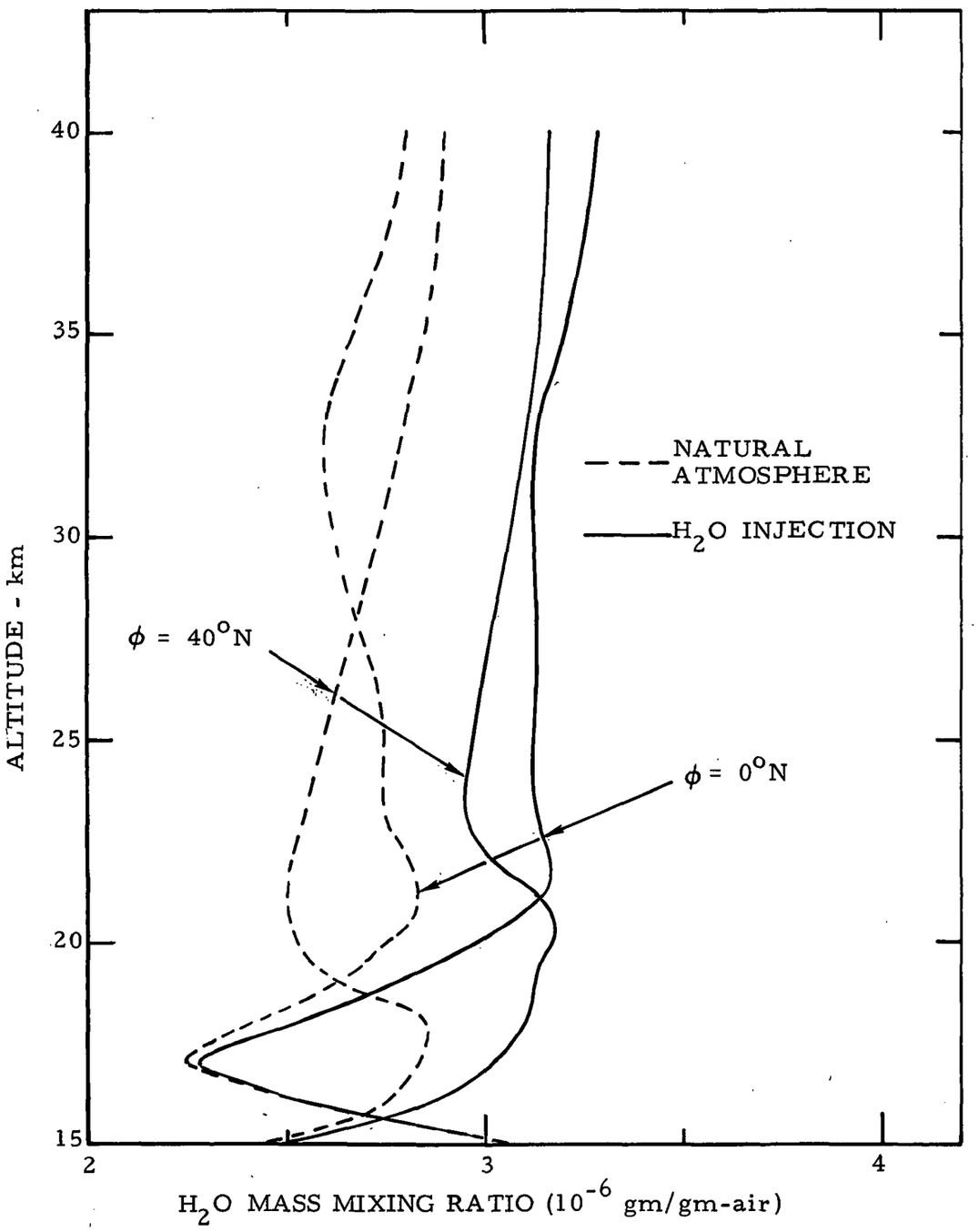

FIG. 28. VERTICAL PROFILES OF WATER FOR H_2O INJECTION DURING THE FALL SEASON

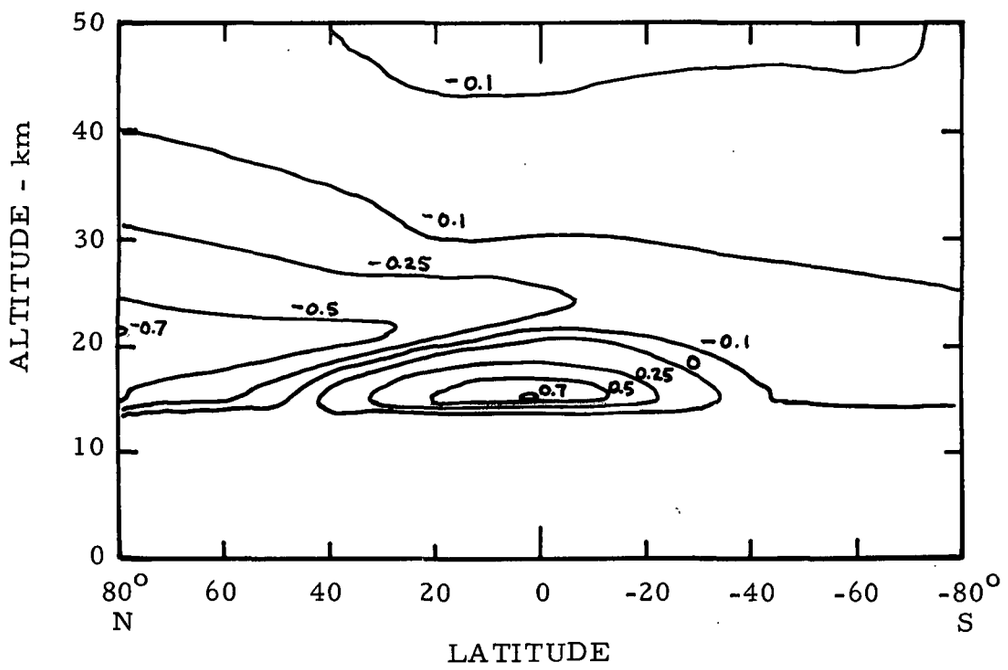

FIG. 29. TEMPERATURE PERTURBATION FOR H_2O INJECTION CASE (°K) DURING THE FALL SEASON

NASA Contractor Report 158945
Distribution List
NAS1-13970

	No. of Copies
NASA Langley Research Center Hampton, VA 23665 Attn: Report & Manuscript Control Office, Mail Stop 180A Linwood B. Callis, Jr., Mail Stop 401B	1 60
NASA Ames Research Center Moffett Field, CA 94035 Attn: Library, Mail Stop 202-3	1
NASA Dryden Flight Research Center P.O. Box 273 Edwards, CA 93523 Attn: Library	1
NASA Goddard Space Flight Center Greenbelt, MD 20771 Attn: Library	1
NASA Lyndon B. Johnson Space Center 2101 Webster Seabrook Road Houston, TX 77058 Attn: JM6/Library	1
NASA Marshall Space Flight Center Marshall Space Flight Center, AL 35812 Attn: Library, AS61L	1
Jet Propulsion Laboratory 4800 Oak Grove Drive Pasadena, CA 91103 Attn: Library, Mail 111-113	1
NASA Lewis Research Center 21000 Brookpark Road Cleveland, OH 44135 Attn: Library, Mail Stop 60-3	1
NASA John F. Kennedy Space Center Kennedy Space Center, FL 32899 Attn: Library, NWSI-D	1

	No. of Copies
National Aeronautics and Space Administration Washington, DC 20546 Attn: ST-5	1
NASA Scientific and Technical Information Facility 6571 Elkridge Landing Road Linthicum Heights, MD 21090	30 + original